

THESIS

DECIPHERING THE LATE JURASSIC PALEOENVIRONMENT THROUGH RE-OS  
ISOTOPE GEOCHEMISTRY OF THE AGARDHFJELLET FORMATION, SVALBARD

Submitted by

Marisa Leigh Connors

Department of Geosciences

In partial fulfillment of the requirements

For the Degree of Masters of Science

Colorado State University

Fort Collins, Colorado

Summer 2017

Master's Committee:

Advisor: Judith Hannah  
Co-Advisor: Holly Stein

Thomas Borch  
Øyvind Hammer

Copyright by Marisa Leigh Connors 2017

All Rights Reserved

## ABSTRACT

### DECIPHERING THE LATE JURASSIC PALEOENVIRONMENT THROUGH RE-OS ISOTOPE GEOCHEMISTRY OF THE AGARDHFJELLET FORMATION, SVALBARD

Accurate interpretations of environmental change throughout Earth's history rely on robust correlations of sedimentary systems. The Late Jurassic has been difficult to correlate regionally and globally due to sparse radiometric ages and lack of cosmopolitan fossils. The rhenium-osmium (Re-Os) geochronometer provides an excellent platform to approach this problem. Re-Os geochemistry provides a way to directly date organic-rich shales which can then be used to: 1) place numerical ages on boreal fossil zones and Geologic Time Scale stage boundaries, 2) correlate with regional or global units, and 3) enhance the understanding of oceanic anoxic events (OAEs) and climactic shifts when paired with additional chemical and lithological data.

The Agardhfjellet Formation of Svalbard, Norway has multiple intervals of organic-rich mudrocks which are ideal for Re-Os geochemistry. Presented here are Re-Os ages which confirm placement of the Agardhfjellet Formation within the Late Jurassic to Early Cretaceous ( $157.9 \pm 2.9$  Ma to  $141 \pm 20$  Ma). We provide an age immediately above the Kimmeridgian-Oxfordian boundary, within the *Amoebocera subkitchini* zone, at  $153.2 \pm 5.0$  Ma in agreement with previous work. Furthermore we present evidence that: (1) the Agardhfjellet Formation was deposited in fluctuating anoxia conditions; (2) increasing initial  $^{187}\text{Os}/^{188}\text{Os}$  ( $0.401 \pm 0.007$  to  $0.577 \pm 0.054$ ) coupled with a decrease in  $\delta^{13}\text{C}_{\text{org}}$  ( $-25.26\text{‰}$  to  $-29.63\text{‰}$ ) through the Late Jurassic

signifies a changing climate represented by an increase continental weathering with a warming climate and/or an increase in continental freeboard.

## ACKNOWLEDGEMENTS

First, I would like to thank my two advisors, Dr. Judith Hannah and Dr. Holly Stein of the Geosciences department at Colorado State University. Their support, patience, and guidance over the past three years have been greatly appreciated. I would like to thank my external committee members Dr. Thomas Borch and Dr. Øyvind Hammer for their understanding in the condensed time-line for defense. I would also like to thank Dr. Holly Stein and Dr. Øyvind Hammer for braving polar bears and the Arctic in January to select the cores for my thesis, in addition to providing the CT scan work through University of Oslo. I would like to thank our research group in the AIRIE (Applied Isotope Research for Industry and Environment) Program for support and help, especially Rich Markey who provided much of the training and background needed to perform Re-Os analyses and complete my thesis.

I would also like to thank Eni Norge, Lundin Petroleum, and Aker BP (formerly Det Norske) for their generous support through the CHRONOS project, and the AAPG Foundation Grants-In-Aid program for their funding support through the Ike Crumbly Minorities in Energy Named Grant – 2015.

I would like to thank my family for always encouraging me to reach for the stars (or Earth!), especially my sister Liana for sharing in the scientific graduate school experience.

Lastly I would like to thank my husband, Gregory Connors for his unending support throughout this process. I could not have done it without you.

## TABLE OF CONTENTS

ABSTRACT.....	ii
ACKNOWLEDGEMENTS.....	iv
LIST OF TABLES.....	vi
LIST OF FIGURES.....	vii
1. INTRODUCTION.....	1
2. GEOLOGIC SETTING.....	4
3. METHODS AND MATERIALS.....	9
Lithological Analyses.....	9
Re-Os Analyses.....	11
External Chemical Analyses.....	12
4. RESULTS.....	14
Core and CT Scan Description.....	14
Thin-Section Petrography.....	17
Re-Os Ages and Osi Results.....	20
Rock-Eval Results.....	24
Stable Isotope Results.....	27
Major and Trace Element Results.....	28
5. DISCUSSION.....	32
Ages.....	32
Local stratigraphy.....	32
Bioturbation and Re-Os ages.....	33
Regional comparisons.....	33
Implications for the Late Jurassic timescale.....	35
Anoxia and Restriction.....	35
Mid-Late Jurassic Climate Shift.....	36
6. CONCLUSIONS.....	39
LIST OF REFERENCES.....	40
APPENDIX A.....	46
APPENDIX B.....	52
APPENDIX C: RE-OS ISOCHRON.....	53

LIST OF TABLES

TABLE 1 –CORE SAMPLE INFORMATION WITH BIOSTRATIGRAPHIC  
CONSTRAINTS .....10

TABLE 2 –UNREFINED AND REFINED RE-OS AGES WITH BIOSTRATICRAPHIC  
AGES .....21

TABLE 3 –GEOCHEMICAL DATA .....46

TABLE 4 –RE-OS TOTAL ANALYTICAL BLANK DATA .....52

## LIST OF FIGURES

FIGURE 1 –REGIONAL AND SAMPLE LOCATION MAPS .....	4
FIGURE 2 –PALEOGEOGRAPHY AND STRATIGRAPHIC RELATIONSHIPS .....	5
FIGURE 3 –COMPOSITE SECTION OF BIOSTRATIGRAPHY AND LITHOGRAPHY .....	7
FIGURE 4 –COMPOSITE IMAGE OF SELECTED LITHOGRAPHIC FEATURES .....	15
FIGURE 5 –PHOTOMICROGRAPHS AND INSET SEM IMAGES .....	18
FIGURE 6 –TWO EXAMPLES OF AGE REFINEMENT TECHNIQUES .....	22
FIGURE 7 –REFINED RE-OS AGES WITH OSI .....	24
FIGURE 8 –GEOCHEMICAL PLOTS WITH DEPTH .....	25
FIGURE 9 –ROCK-EVAL DATA PLOTS.....	26
FIGURE 10 –REDOX PROXY PLOTS.....	29
FIGURE 11 –COMPOSITE OSI FROM MIDDLE JURASSIC TO EARLY CRETACEOUS...	37

## 1. INTRODUCTION

Accurate interpretations of Earth's paleoenvironmental and biological changes throughout time rely heavily on robust correlations of sedimentary systems. In some segments of Earth time, i.e. Late Jurassic, correlation issues arise from lack of tie-points such as cosmopolitan fossils and/or sparse radiometric ages. The rhenium-osmium (Re-Os) geochronometer provides a means of directly dating organic rich mudrocks (ORM) which, in turn, validates correlations in these previously problematic systems.

Re-Os geochemistry is increasingly useful in the study of ORM (Ravizzia and Turekian, 1989; Creaser et al., 2002; Selby and Creaser, 2003a; Cohen, 2004; Kendall et al., 2009). Several applications of the Re-Os system, in coordination with other trace metal and isotopic data, include: (1) adding precise numerical ages to system and stage boundaries (Selby and Creaser, 2003b; Selby, 2007; Xu et al., 2009), (2) providing insight into the status of anoxia within a basin (Turgeon and Creaser, 2008; Georgiev et al., 2012; Georgiev et al., 2017), (3) providing evidence of changing climactic conditions through use of the calculated initial  $^{187}\text{Os}/^{188}\text{Os}_i$  ( $\text{Osi}$ ) parameter (Ravizzia et al., 2001; Finlay et al., 2010; Georgiev et al., 2011; Xu et al., 2013), and (4) making intra- and inter-basinal correlations (Rooney et al., 2010; Markey et al., 2017).

The Re-Os system has been proven intact through a variety of potentially disruptive processes such as hydrocarbon maturation and migration (Creaser et al., 2002) and high-temperature, contact metamorphism (Kendall et al., 2010; Kendall et al., 2011). The ideal sedimentary candidates for Re-Os geochemistry tend to be extremely fine-grained, which generally limits fluid migration, a major cause of disruption to the Re-Os system. Isochroneity in the Re-Os system is an effective indicator of preservation of primary chemical characteristics of ORM which is critical in robust interpretation (Georgiev. et al., 2012). However, there are still

processes which can reset or overprint the Re-Os systematics in ORM (Yang et al., 2009; Kendall et al., 2009; Rooney et al., 2011; Mahdaoui et al., 2015). These can produce non-isochronous results. In this study, a combination of chemical and lithological evidence is used to identify potential outliers and/or disturbed data points, thereby refining previously non-isochronous results and gaining useful information through Re-Os geochronology

The Agardhfjellet Formation of Svalbard, Norway offers appropriate materials for using rhenium-osmium (Re-Os) geochemistry to enhance understanding of Late Jurassic paleogeography and paleoenvironment. First, Re-Os geochemistry of regional correlatives to the Agardhfjellet Formation, including the prolific source rocks of the Hekkingen Formation (southern Barents and Norwegian Seas), the Kimmeridge Clay (North Sea and the United Kingdom), and the Staffin Formation (Isle of Skye, UK) have been characterized by previous studies (Cohen et al., 1999; Selby, 2007; Markey et al., 2017; Georgiev et al., 2017). These provide regional, chronostratigraphic benchmarks for correlation and an opportunity to constrain the ages of Late Jurassic stage boundaries that are currently based on bio- and magnetostratigraphy (Gradstein et al., 2012).

Second, sparse radiometric ages of the Late Jurassic coupled with limited connectivity between Tethyan, Proto-Pacific and Boreal marine realms have prevented global correlation of fossils, specifically ammonites, which provide the best-defined fossil zones for the Late Jurassic (Cope, 2008; Gradstein et al., 2012). While individual ammonite zones have been well characterized, they have limited overlap not only inter-realm but intra-realm (Page, 2008). The biostratigraphy of the Agardhfjellet Formation has been well defined by previous workers (Wierzbowski et al., 2011; Koevoets et al., 2016). Using this biostratigraphy in conjunction with Re-Os geochronology can tie Boreal ammonites into the global time-scale.

Third, combining Re-Os geochemistry of the Agardhfjellet Formation with additional chemical and lithological data will enhance paleoenvironmental interpretations of the Boreal realm, including the duration of local anoxia and changes in paleoclimate. The record of Middle to Late Jurassic climate change has been documented in correlative units by multiple workers (e.g. Ditchfield, 1997; Abbink et al., 2001; Gröcke et al., 2003; Georgiev et al., 2017). This growing body of evidence shows a period of warming, increased chemical weathering, and overall sea-level rise on a global scale. In order to understand how the Boreal realm in Svalbard fits with these trends it is imperative to have robust correlations; these can be provided by Re-Os geochemistry.

## 2. GEOLOGIC SETTING

The Agardhfjellet Formation is defined on the high-arctic archipelago of Svalbard, Norway (Fig. 1A), marking the base of the Middle Jurassic to Early Cretaceous Adventdalen Group in central and southwestern Spitsbergen (Dypvik et al., 1991; Mørk et al., 1999).

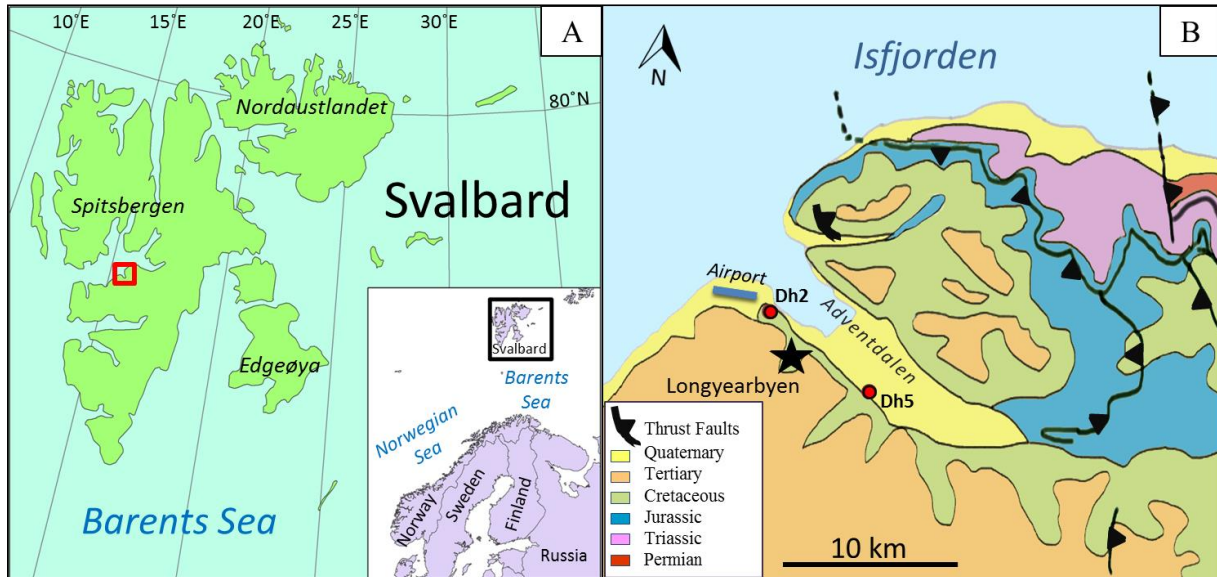


**Figure 1-Regional and Sample Location Maps.** A) Location map showing Svalbard (black outline) and study area (red outline). B) Locations of Longyearbyen CO<sub>2</sub> Lab drill hole 2 (Dh2) and drill hole 5 (Dh5) with generalized surficial geology after Braathen et al., 2012.

The ORM of the Agardhfjellet Formation were deposited throughout the Middle to Late Jurassic in a shallow to deep, marine shelf setting off the coast of present-day Greenland (Dypvik et al., 1985, 2002) (Fig. 2A). The Boreal region as a whole experienced intermittent anoxia throughout the Middle to Late Jurassic (Dypvik, 1985; Nagy et al., 1988) leading to the deposition of thick packages of organic-rich sediments within the Agardhfjellet Formation and its correlatives including the Måsnøkan, Fuglen, and Hekkingen Formations of Barents and Norwegian Seas (Fig. 2B).

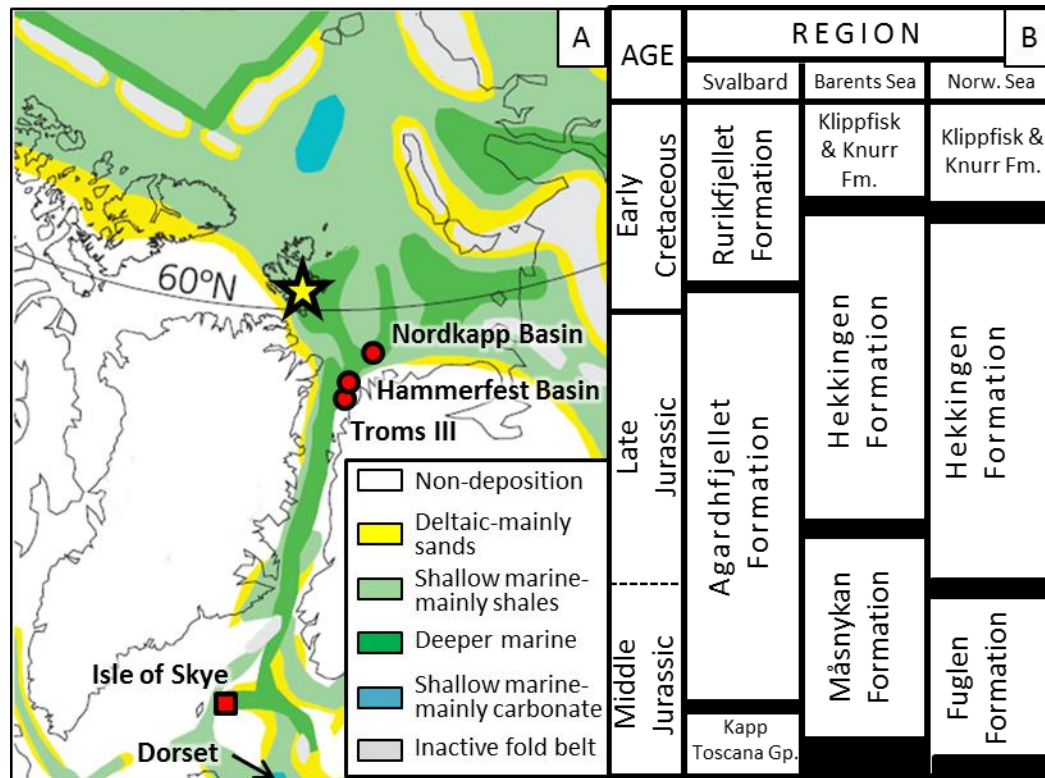


**Figure 2-Paleogeography and Stratigraphic Relationships.** A ) Paleogeographic reconstruction (after Torsvik et al., 2002) with Re-Os study locations. Star – this study. Circles – previous AIRIE studies in the Hekkingen Formation (Markey et al., 2016; Georgiev et al., 2016) Square – Staffin Bay Formation (Selby, 2007). Arrow points off-image to Kimmeridge Clay at Dorset (Cohen et al., 1999). B) Regional stratigraphic correlations based on Dypvik et al. 2002 and Smelror et al., 2001.

Spitsbergen and adjacent areas experienced a variety of igneous and tectonic activity after the deposition of the Agardhfjellet Formation. Cretaceous dolerite sills related to the High Arctic Large Igneous Province are present in Dh5; most, however, intrude the Triassic and Middle Jurassic units more than 200 m below the Agardhfjellet Formation. This activity led to regionally elevated geothermal gradients estimated up to 50° C/km (Senger et al., 2014a; Senger et al., 2014b; Marshall et al., 2015). The present-day geothermal gradient has been measured at 40° C/km (Braathan et al., 2012). The Agardhfjellet Formation and overlying Rurikfjellet Formations were deposited in a tectonically quiet basin. Throughout the Paleogene, however, transpressional deformation related to the opening of the Greenland Sea generated large thrust belts and created the Tertiary Central Basin on Spitsbergen (Braathen et al., 1999). In the early Oligocene the

Agardhfjellet Formation reached its peak depth of greater than 3000 m (Michelsen and Khorasani, 1991) followed by relatively rapid exhumation and uplift to its present depth within the Tertiary Central Basin at Longyearbyen.

Core segments for this study were collected in organic-rich mudstone and claystone intervals of the Agardhfjellet Formation from two wells of the Longyearbyen CO<sub>2</sub> Lab project near Longyearbyen, Svalbard. The Agardhfjellet Formation outcrops to the north and east of Longyearbyen whereas in the study area it is in the subsurface (Fig. 1B). For the CO<sub>2</sub> Lab project two clusters of wells were drilled seven kilometers apart to test for potential CO<sub>2</sub> storage in the Early Jurassic Kapp Toscana Group, which underlies the Agardhfjellet Formation. Core was chosen from one well in each cluster: Dh2 near the Svalbard airport and Dh5 to the south of Longyearbyen (Fig 1B). At Dh2 the Agardhfjellet Formation spans a depth of 732 m to 481 m. At Dh5 the base of the Agardhfjellet is placed at 671 m depth while the top is not well-defined due to a thick interval of diamictite (Koevoets et al., 2016). Within the study area the Agardhfjellet Formation dips to the NW so that correlative strata in Dh2 are 60 m deeper than Dh5 (e.g. Dh2 660 m  $\approx$  Dh5 600 m; Fig. 3). A regional detachment zone has been identified in the uppermost Agardhfjellet Formation within both drill holes (Braathen et al., 2012), but this starts several 10's of meters above the shallowest sample collected for this study.

The Agardhfjellet Formation at Longyearbyen is divided into four members including, from base to top, the Oppdalen, Lardyfjellet, Oppdalssåta, and the Slottsmøya (Dypvik et al., 1991; Koevoets et al, 2016). All members are recognized in the drill core (Fig. 3). The Oppdalen Member, which unconformably overlies the coarse-grained Kapp Toscana Group, consists of silty to sandy mudstones with intermittent siderite horizons. *Kepplerities svalbardensis* was identified within the lower Oppdalen Member (Fig. 3) making it uppermost Bathonian in age.

The Lardyfjellet Member is chiefly organic-rich black shale with intermittent siderite horizons. It coarsens upward at the top into greyish, siltier layers. Within the Lardyfjellet Member there are abundant fossils including the fish bones, bivalves, microfossils, and the Lower Kimmeridgian ammonite *Amoeboceras subkitchini* (Fig.3).

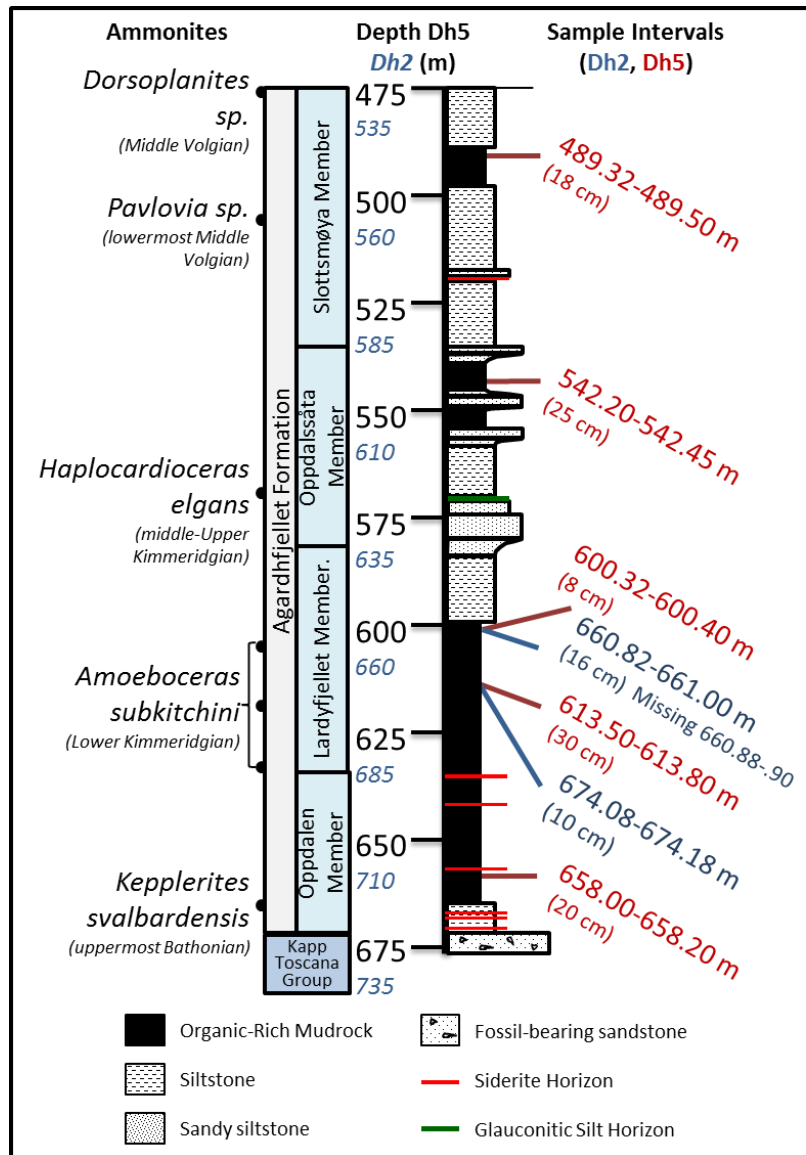


**Figure 3-Composite section of Biostratigraphy and Lithostratigraphy.** Lithostratigraphy and biostratigraphy of the Agardhfjellet Formation from Dh5 and Dh2 (after Hammer, written communication, 2014; Koevoets et al., 2016). Core intervals used for analyses in this study marked on right. Length of collected core sample in parentheses below intervals.

The Oppdalssåta Member is the most varied lithologically. It consists of several coarsening up sequences which grade from shale with variable organic material into sandy siltstones with intermittent glauconitic horizons. The Upper Kimmeridgian ammonite, *Amoeboceras elegans*, was identified in the Oppdalssåta Member (Fig.3). The Slottsmøya Member has the fewest organic-rich intervals and is chiefly grey shale with intermittent siderite horizons. The Middle Volgian ammonites of *Pavlovia sp.* and *Dorsoplanities sp.* are found in the Slottsmøya as well as plentiful bivalves, fish bones, and woody debris (Hammer, 2014; Koevoets et al., 2016; Fig. 3). The Volgian stage is defined from Boreal fossils and correlative to the Tithonian and lowermost Berriasian stage. The Slottsmøya member is unconformably overlain by the widespread Myklegardfjellet bed of the Early Cretaceous Rurikfjellet Formation.

### 3. METHODS AND MATERIALS

#### **Lithological analyses**

Seven segments of whole drill core ranging from 8 to 30 cm in length were chosen from organic-rich shale intervals of the Agardhfjellet Formation in Dh2 (N=2) and Dh5 (N=5) by Dr. Holly Stein (Table 1). Segments were selected for lack of evidence of bioturbation (well-laminated samples), lack of visible structural deformation (folding, faulting, joints), and potential for high organic matter (black shale). Identified segments were prioritized for proximity to: (1) potential stage boundaries (e.g., Oxfordian-Kimmeridgian), (2) proximity to upper and lower formational boundaries or (3) an identified fossil zone (e.g., *A. subkitchini*). Dr. Øyvind Hammer at the University of Oslo provided both biostratigraphy and x-ray computed tomographic scans (CT) for core segments. Core was then taken to Colorado State University for sampling and Re-Os analyses.

Whole core segments were photographed and described before and after splitting with a diamond-tipped saw. One half of each core segment was saved for reference while the other half was used for sampling. Four polished thin-sections (one each from Dh2-660, Dh2-674, Dh5-600 and Dh5-613) were made for detailed petrographic study of correlative segments of Dh5 and Dh2. Optical microscopy was performed at Colorado State University. Framboid size ranges were determined by reflected light microscopy and measurements made with digital imager calibrated using ProgRes CapturePro 2.8.8 software. SEM and electron microprobe analyses were performed at the University of Oslo. SEM and microprobe were used to identify compositions of select grains. Multiple samples < 1 cm thick were selected from each core

**Table 1: Core and Sample Information with Biostratigraphic Constraints.**

Drill Hole	Segment ID (hole-depth)	depth interval (m)	Total Length of core (cm)	Samples taken	Agardhfjellet Member	Biostratigraphic age	Reference Fossils
Dh5	Dh5-489	489.32-489.50	18	5	Middle Slottsmøya	Middle Volgian	Between <i>Dorsoplanites sp.</i> and <i>Pavlovia sp.</i>
Dh5	Dh5-542	542.20-542.42	22	5	Upper Oppdalssåta	Kimmeridgian-Volgian (?)	Between <i>Amoeboceras elgans</i> and <i>Dorsoplanites sp.</i>
Dh5	Dh5-600	600.32-600.40	8	5	Upper Lardyfjellet	late-Early Kimmeridgian	<i>Amoeboceras subkitchini</i>
Dh5	Dh5-613	613.50-613.80	30	8	Upper Lardyfjellet	mid-Early Kimmeridgian	<i>Amoeboceras subkitchini</i>
Dh5	Dh5-658	658.00-658.20	20	5	Middle Oppdalen	Bathonian-Callovian (?)	Between <i>Kepplerites (S.) svalbardensis</i> and <i>Amoeboceras subkitchini</i>
Dh2	Dh2-660	660.82-661.00 <sup>A,B</sup>	6, 10 <sup>B</sup>	8	Upper Lardyfjellet	late-Early Kimmeridgian	<i>Amoeboceras subkitchini</i>
Dh2	Dh2-674	674.08-674.18 <sup>A</sup>	10	5	Upper Lardyfjellet	mid-Early Kimmeridgian	<i>Amoeboceras subkitchini</i>

A-Dh2 intervals are equivalent to Dh5 depth plus 60 m (e.g. Dh2 660 m = Dh5 600 m)

B-Interval from 660.88-660.90 m taken for ammonite study by Dr. Øyvind Hammer and his student Maayke Koevoets.

C-(Hammer, 2014; Koevoets et al., 2016)

segment for Re-Os analyses as well as additional geochemical analyses. Individual samples of 5 to 10 grams were either taken along parting laminations or, in the case of well indurated samples (Dh2), cut using a diamond tipped saw. These samples were rinsed with DI water and dried before pulverizing using a corundum mortar and pestle and an agate ball mill to produce a fine, homogenized powder. The powder was split for Re-Os, trace element, total organic carbon (TOC), Rock-Eval pyrolysis, and stable isotopes analyses.

### **Re-Os Analyses**

Rhenium-osmium geochemistry was performed at the AIRIE (Applied Isotope Research for Industry and Environment) Program at Colorado State University in accordance with previously defined procedures described briefly below (Georgiev et al., 2015). A total of 41 powdered samples, ranging from 300-500 mg, were used to obtain the seven isochrons reported here. A calculated amount of Re and Os spike solutions, enriched in  $^{185}\text{Re}$  and  $^{190}\text{Os}$  respectively, were added to samples prior to digestion for subsequent calculation of sample Re and Os concentrations by isotope dilution. Samples were digested in 11 mL of  $\text{CrO}_3\text{-H}_2\text{SO}_4$  for 48 hours in sealed Carius tubes at  $240^\circ\text{C}$ . Chemical separation and purification of Re and Os were accomplished using H Br extraction and microdistillation (Os), followed by anion exchange column separation (Re). Re and Os were loaded onto outgassed, high-purity, platinum filaments for analysis with a barium activator solutions,  $\text{Ba}(\text{NO}_3)_2$  for Re and  $\text{Ba}(\text{OH})_2$  for Os. Isotopic ratios were measured by negative thermal ionization mass spectrometry (NTIMS) using Triton mass spectrometers at the AIRIE Program, CSU. Each batch of sample measurements also included a total analytical blank (TAB) and in-house standards.

Measured isotopic ratios are corrected for oxygen isotope contributions, mass fractionation (Os), TAB contributions, and spike contributions. Re contributions from blanks

ranged from 0.05% to 4.9% with a mean of 0.8%. Os contributions from blanks ranged from 0.062% to 0.31% with a mean of 0.15%. Blank contributions to individual samples can be seen in appendix A with blank information in appendix B. Re and Os standards for these samples are:  $^{185}\text{Re}/^{187}\text{Re} = 0.59717 \pm 0.00056$ ,  $1\sigma$ ,  $n = 9$ ;  $^{187}\text{Os}/^{188}\text{Os} = 0.12375 \pm 0.00016$ ,  $1\sigma$ ,  $n = 9$ ). These are statistically consistent with AIRIE long-term averages.

Uncertainties calculated for Re-Os analyses include weighing errors, errors on spike calibrations, errors on measured ratios, an error magnifier based on spiking ratios, and uncertainty in blank corrections. Isochrons were calculated using Isoplot 3.75 (Ludwig, 2012). Resulting uncertainties in ages are based on the fit of the regressed line. Uncertainty in the  $^{187}\text{Re}$  decay constant ( $1.666 \times 10^{-11} \text{ yr}^{-1} \pm 0.31\%$ ) was added to reported ages.

### **External Chemical Analyses**

Leco TOC and Rock-Eval pyrolysis results were obtained from Geomark Research Inc. TOC, S1, S2, S3, and TMax were reported for 41 samples along with a calculated vitrinite reflectance (from TMax) and calculated percent carbonate from loss of mass after initial treatment with HCl. The S1 peak represents the free hydrocarbons in rock. The S2 peak represents the volume of hydrocarbons produced during the pyrolysis process which is used to calculate the hydrogen index (HI) and is an estimate of hydrocarbon generation potential. The S3 peak represents produced  $\text{CO}_2$  from pyrolysis and is used to calculate the oxygen index (OI). TMax is determined from the temperature at the apex of the S2 peak.

Stable isotope analyses for selected samples were obtained from Iso-Analytical Limited, Crewe, United Kingdom. Analyses were performed using an Elemental Analyser-Isotope Ratio Mass Spectrometer (EA-IRMS) for bulk  $\delta^{15}\text{N}$  ( $n=14$ ),  $\delta^{34}\text{S}$  ( $n=15$ ), and organic  $\delta^{13}\text{C}$  ( $n=15$ ); and a Continuous Flow- Isotope Ratio Mass Spectrometer (CF-IRMS) for carbonate  $\delta^{18}\text{O}$  and  $\delta^{13}\text{C}$

(n=12). Measurements were reported relative to V-PDB for  $\delta^{18}\text{O}_{\text{carb}}$ ,  $\delta^{13}\text{C}_{\text{carb}}$ ,  $\delta^{13}\text{C}_{\text{org}}$  V-CDT for  $\delta^{34}\text{S}$ , and air for  $\delta^{15}\text{N}$ .

Selected major and trace element analyses were obtained commercially through Activation Laboratories, Ontario, Canada. The Ultratrace 6 method was used to obtain 61 trace and major element concentrations from 41 shale samples. Samples were processed using multi-acid total digestion and measured using ICP-AES for major elements and scandium and ICP-MS for remaining trace elements. Details of the 61 elements can be found in appendix A.

## 4. RESULTS

### Core and CT Scan Descriptions

Descriptions for the Dh5 core begin with the uppermost sample from the Slottsmøya Member (Dh5-489) and ends with the lowest sample (Dh5-658) from the Oppdalen Member. Where present, all laminations are perpendicular to the length of the core.

Dh5-489, in the upper-middle Slottsmøya Member, is a dark-grey, moderately-indurated, silty, claystone with trace visible (< 1 mm) pyrite, mostly associated with partial carbonate replacement. Although bedding is not observable in hand sample, CT scans show minor laminations visible with some scattered framboids and agglutinated forams.

Dh5-542, in the upper Oppdalssåta Member, is a dark grey to black, moderately-indurated mudstone. Small pyrite nodules/framboids (< 1 mm), *Teichnitas* burrows, and agglutinated foraminifera are visible both in CT scan and in hand sample (Fig. 4A). These are most prevalent between 542.28 m and 542.40 m. Small onychites (> 1 cm) are also present in some laminae. A slickenside is visible at the top of the core segment (542.28 m, Fig. 4B).

Dh5-600, in the upper Lardyfjellet Member, is a black to dark grey, moderately-indurated, clay-rich mudstone. Discontinuous laminations are difficult to discern in hand sample. In CT scans, laminations are highly visible and generally defined by agglutinated foraminifera and pyrite nodules.

Dh5-613, in the middle Lardyfjellet Member, is a black to dark grey, well-indurated, mudstone. Several wavy, continuous to discontinuous, silty, laminae are present in the upper ~10 cm and decrease in frequency as well as thickness (< 1 mm) with increasing depth. Macrofossils are present and include a bivalve (10-12 mm) replaced by pyrite at 613.62 m, and

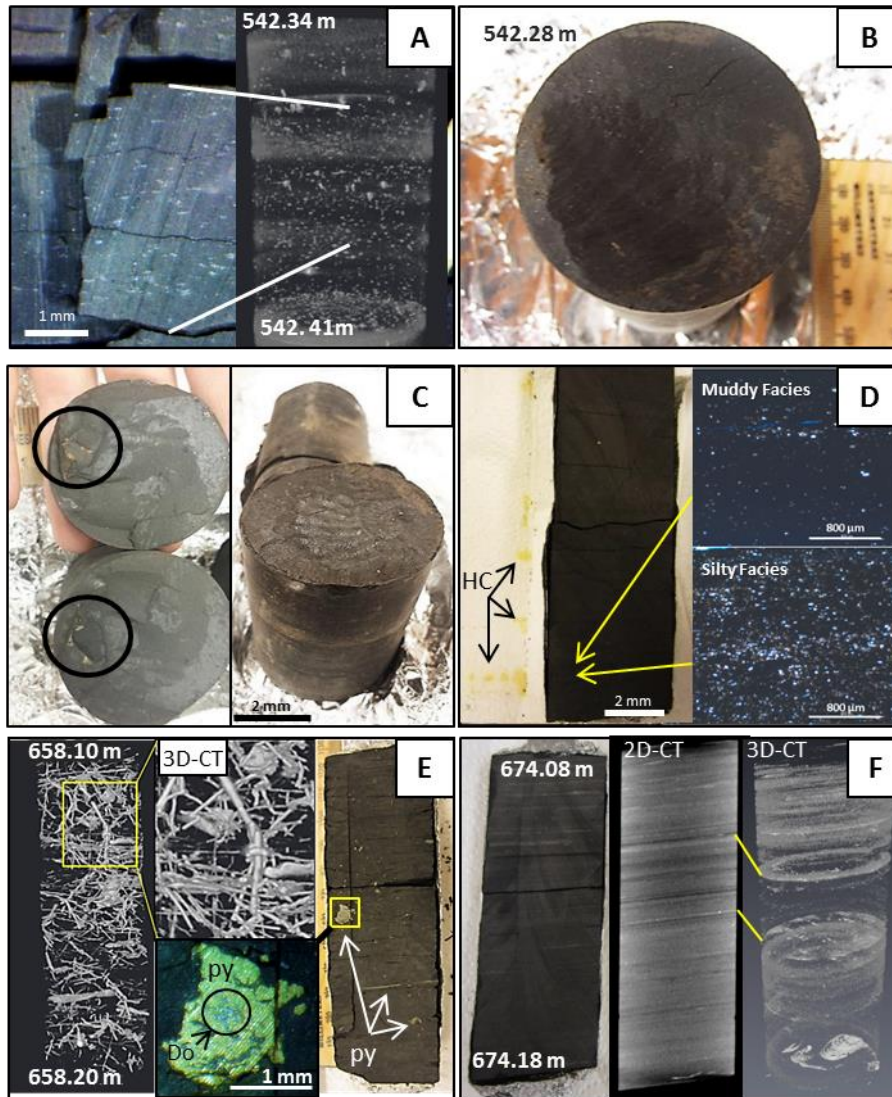


**Figure 4-Composite image of selected lithographic features.** A) Agglutinate foraminifera from Dh5-542 comparing photographed core (left) to CT scan (right). B) Slickenside located at 542.28 m in Dh5. C) Pyritized fossils (black circles) at 613.32 m and *A. subkitchini* mold at 613.68 m (right) from Dh5. D) Hydrocarbon (HC) leached into paper towel from silty facies and fractures from Dh5-613. E) Pyritized and dolomitized burrows from Dh5-658 in 3D-CT scan (left) and slabbed core (right). F) Laminations of Dh2-674 in slabbed core and CT scans. CT scans are set for different contrasts. In both images laminations are easily visible sub-parallel to cross-section of core. A Fe-dolomite bivalve is visible in the lowest portion of the 3D-scan.

the imprint of an ammonite (*A. subkitchini*) at 613.68 m (Fig. 4C). Several fractures sub-parallel to core and a semi-vertical fracture developed after sawing. A few of these fractures within siltier laminations show hydrocarbon leaching into paper towels after drying from sawing process (Fig. 4D).

Dh5-658, in the middle Oppdalen Member, is a fissile, dark grey, silty-claystone. Pyrite is highly abundant throughout this core, chiefly replacing burrows. CT scans show that burrows are predominantly horizontal to sub-horizontal single-track as well as a few vertical, single-track burrows, and few branching-downward burrows (Fig. 4E). These have been interpreted as *Planolites* and possible *Chondrites* although branching is rare. Several of the larger burrows have a dolomite core indicating only partial pyritization took place (Fig. 4E). The Dh5-658 core segment comes from an interval below a siderite hardground and itself has been cemented by siderite. This has prevented significant compaction which is also reflected in the preserved geometries of the burrows.

Both segments of studied core from Dh2 come from the Lardyfjellet Member of the Agardhfjellet Formation, and are correlative to the Lardyfjellet Member core in Dh5 (Fig. 3). Dh2-660 is a black to dark grey, well-indurated, silty-claystone. Parallel, continuous to discontinuous, silty laminations are readily visible in hand-samples and in CT scan. Laminae are at an angle of  $\sim 95^\circ$  to the core length. Several macrofossils, most likely bivalves, are present in the lower 10 cm, parallel to bedding. These are generally dolomite with or without partial pyritization. A 2 cm gap in the core between the lower and upper segment was taken by other workers to identify a bivalve which had been buried in an upright position. Above this interval, the upper 6 cm of core lacks obvious macrofossils.

Dh2-674 is a black to dark grey, well-indurated, silty claystone. Thin, continuous, silty laminations at  $\sim 85^\circ$  to the length of the core are well expressed in both hand sample and CT scan at (Fig. 4F). While the core as a whole coarsens upward, individual laminations show fining upwards. A slickenside appears at the top of the core segment, 674.08 m.

## Thin-Section Petrography

Thin-sections of the Lardyfjellet Formation reveal detailed information through optical microscopy and additional electron microprobe and scanning electron microscope (SEM) analyses. The following descriptions compare findings from correlative units in Dh2 and Dh5.

The upper correlative intervals are Dh2 660.83 m- 660.865 m and Dh5 600.32 m- 600.355 m. In both cases, thin-sections were taken near the top of an identified organic-rich mudstone below the transition to the coarser upper siltstone of the Lardyfjellet Member. Distinct muddy and silty facies were identified within the Dh5-600 thin section, similar to those in Fig 4D. The muddy facies is poorly-laminated with ~1-5% medium silt to very-fine sand-sized clasts. Clasts are primarily subangular to subrounded quartz and muscovite. The silty facies is a silty claystone with 10-15% clasts. Clasts are ~5% agglutinated foraminifera and 10% clastic grains (angular to subangular quartz, muscovite, and trace detrital intraclasts of smectite and illite). In both facies, muscovite flakes are parallel to sub-parallel to bedding. Pyrite is present in two main forms: framboids and replaced microfossils. Disseminated framboids occur throughout the thin sections and clustered framboids appear near algal material and microfossils (similar to Fig. 5A, B). Framboids from clusters average  $16.8 \pm 10.7 \mu\text{m}$  ( $n=92$ ;  $2\sigma$ ), whereas disseminated framboids are generally smaller at  $11.2 \pm 9.5 \mu\text{m}$  ( $n=40$ ;  $2\sigma$ ).

Facies in Dh2-660 are similar to Dh5-600 although overall Dh2-660 has a higher proportion of silt. Again, two facies are recognizable: a muddy facies and a silty facies. The muddy facies is 5-10% fine silt to very-fine sand, 1-5% organic material and the remaining fraction clay-sized material. Silt and sand-sized clasts are angular to subangular quartz and muscovite, bioclasts, and trace detrital clays including smectite. The silty facies is generally 10-20% fine-silt to very-fine sand of similar composition to the muddy facies, with 1-2% organic

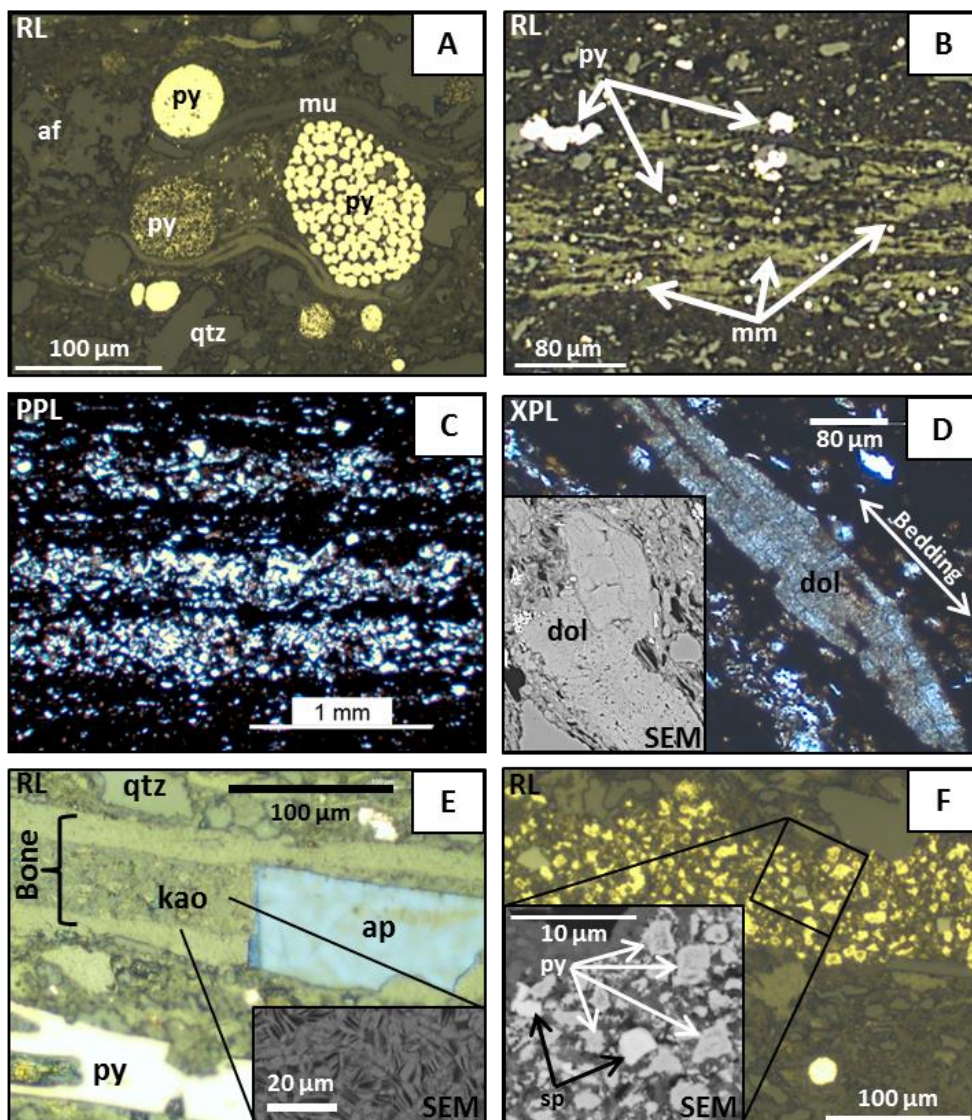


**Figure 5-Photomicrographs and inset SEM images.** A) Pyrite framboid cluster in Dh2-660. Elongate grains are compacted around cluster. B) Microbial mats in Dh2-613 with associated pyrite. C) Sub-mm siltstone laminations within the silty facies of Dh2-674. D) Bioclasts from Dh2-674 which have been recrystallized as Fe-dolomite. E) Bone fragment with infilling kaolinite and apatite, and a pyritized bioclast in Dh2-674. F) Cluster of pyrite and sphalerite from Dh2-674. Pyrite shows overgrowth textures (See “Thin-section petrography” for more detail). Key abbreviations: py-pyrite, mu-muscovite, qtz-quartz, af-agglutinated foraminifera, mm-microbial mat, dol-dolomite, kao-kaolinite, ap-apatite, sp-sphalerite, RL-reflected light, PPL-plain polarized light, XPL-crossed-polarized light, SEM-scanning electron microscopy photograph.

material and the remaining fraction clay-sized material. This facies also shows discontinuous, thin (10-100  $\mu\text{m}$ ) laminations of 40-50% silt-sized particles with the remainder clay and organic material. Silt-rich laminations commonly show scoured contacts with underlying beds. Pyrite is in the form of framboids with few microfossils. In contrast to Dh5-600, disseminated framboids

are dominant. Disseminated framboids are  $8.9 \pm 8.5 \mu\text{m}$  ( $n=99$ ;  $2\sigma$ ) while clustered framboids are  $30.8 \pm 23.2 \mu\text{m}$  ( $n=24$ ;  $2\sigma$ ). Phosphatic bone fragments of up to  $500 \mu\text{m}$  in length, most likely from fish, are present throughout section but more concentrated in the silty facies.

The second pair of correlative samples is Dh5 613.765-613.80 m and Dh5 674.095-674.125 m. Dh5-613 shares a similar silty facies to Dh5-600, however there are differences in the muddy facies. The muddy facies is  $<1\%$  medium to very-fine silt consisting of sub-angular to sub-rounded quartz and trace muscovite. Several thin layers of discontinuous microbial mats that host most of the framboids in this section are present in the muddy facies (Fig. 5B). Disseminated framboids exist throughout both facies although no significant size difference occurs between these and the mat-hosted framboids. Combined, framboids have a mean diameter of  $9.1 \pm 5.2 \mu\text{m}$  ( $n=149$ ;  $2\sigma$ ). Carbonate bioclasts and long fragments of bone (probably fish) are present in both facies and lie parallel to sub-parallel to laminations.

Dh2-674 has two facies (muddy and silty) but overall is much siltier than Dh5-613. The muddy facies is 15-30% silt to very-fine sand. Sub-angular to sub-rounded quartz makes up a majority of the clasts with trace muscovite and detrital clays. Microbial mats define several continuous to discontinuous laminations within the muddy facies. The silty facies occurs in discrete, continuous to discontinuous laminations, usually scoured into the muddy facies (Fig. 5C). These laminations are 50-80% fine silt to fine sand with an average of coarse silt. Clasts are chiefly angular to sub-rounded quartz with muscovite and detrital clay-intraclasts. Bioclasts are common in both facies. Several macrofossils (2-3 mm) are recrystallized as ferroan dolomite while microfossils tend to be replaced by pyrite (Fig. 5D and, E). Bone fragments typically have pore spaces filled with kaolinite or crystalline apatite (Fig. 5E). Framboids occur as disseminated grains ( $12.4 \pm 8.0 \mu\text{m}$ ;  $n=74$ ;  $2\sigma$ ) and in clusters around microbial mats ( $17.0 \pm 9.6 \mu\text{m}$ ;  $n=36$ ;

2 $\sigma$ ). One cluster of sulfides at ~674.087 m displays a different texture than previously encountered (Fig. 5F). Sphalerite and pyrite are both present. The internal structure of the pyrite is pitted whereas the rim is unblemished. From SEM analyses, pyrite within this cluster shows measureable amounts of Ni and Cu whereas framboids nearby do not. Associated sphalerite houses measureable Cd.

### **Re-Os Ages and Osi Results**

Seven Re-Os isochrons are reported for the Agardhfjellet Formation (Table 2). These isochrons have been refined to omit identifiable outliers using a combination of three methods. The first method involves identification of samples located next to geologically induced fractures which provide potential conduits for fluids in the subsurface. In the core extraction and slabbing processes, fractures can be induced which are not geological in nature. These induced fractures do not contribute to Re-Os disrupting fluid movement, and therefore can be used confidently in the sampling process. CT scans were used to locate bedding plane fractures, produced by relieving over-burden upon core extraction, and to identify slabbing-induced fracturing as the core was scanned intact. For example, sample 489.33 m from Dh5 was found to be located on a geologic fracture (Fig. 6A). Removal of this point decreased the uncertainty on the Re-Os age by 10 Ma (Fig. 6B and, C). The second method is to identify sub-mm changes in lithology. The grain size of ORMs generally provide baffles to fluid movement. Because of this, even the thinnest siltstone intervals can provide potential conduits for fluid movement (ex. Fig. 4D) that can affect or over-print the depositional Re-Os signature within sub-mm laminae. The third method of refinement is to identify chemical outliers, generally within the redox sensitive elements. Outliers which have significantly different chemical signatures than the surrounding

**Table 2: Unrefined and Refined Re-Os ages with Biostratigraphic Ages.** Biostratigraphic ages are ammonite-based and inferred from the GTS 2004 and GTS 2012. Samples are listed in restored stratigraphic order. Isochrons were created using Isoplot 4.15 (Ludwig, 2008) and are shown in Appendix C.

Segment ID	Unrefined Age (Ma) <sup>A,C</sup>	err (Ma)	Os <sub>i</sub>	err	Refined Age (Ma) <sup>B,C,D</sup>	err (Ma)	Os <sub>i</sub>	err	sample(s) excluded (m)	Biostratigraphic age from GTS 2012 (Ma)	Biostratigraphic age from GTS 2004 (Ma)
Dh5-489	<i>144</i>	30	0.565	0.080	<i>141</i>	20	0.577	0.054	489.33	~146-149	~146-149
Dh5-542	<i>149.8</i>	7.8	0.668	0.054	<i>149.8</i>	7.8	0.668	0.054	none	~152	~149-153
Dh5-600	<b>131.9</b>	<b>7.3</b>	0.638	0.046	<b>131.9</b>	<b>7.3</b>	0.638	0.046	none	~154	~154-153
Dh2-660	<i>148</i>	16	0.55	0.11	<i>150.9</i>	4.7	0.526	0.032	660.96, 660.955, 660.915	~154	~154-153
Dh5-613	<i>144</i>	16	0.523	0.09	<b>145</b>	<b>2.0</b>	0.525	0.011	613.70, 613.78	~156	~154-153
Dh2-674	<b>153.2</b>	<b>5.0</b>	0.473	0.038	<b>153.2</b>	<b>5.0</b>	0.473	0.038	none	~156	~154-153
Dh5-658	<b>157.9</b>	<b>2.9</b>	0.4015	0.0065	<b>157.9</b>	<b>2.9</b>	0.4015	0.0065	none	~161-164	~164.7-154

A-Unrefined age refers to isochron age with all NTIMS measured samples

B-Refined age refers to best isochron age with justifiable omitted samples. See text (Re-Os Ages and Os<sub>i</sub> Results) for discussion

C-Italics for Model 3 age, Bold for Model 1 age

D-Non-depositional ages in grey. See text (Re-Os Ages and Os<sub>i</sub> Results) for details.

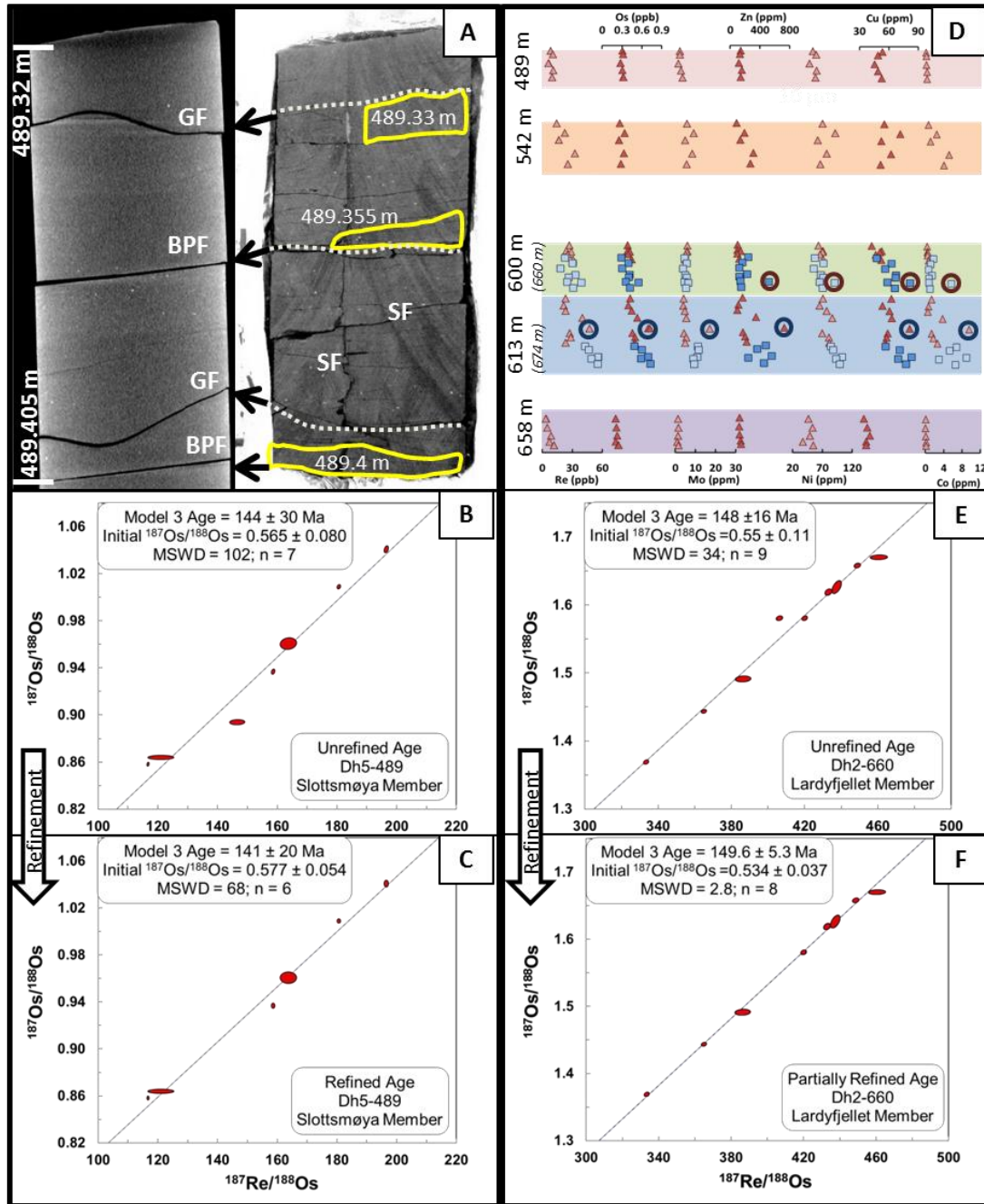


**Figure 6-Two Examples of Age Refinement Techniques** (See “Re-Os Ages and Osi Results” for discussion) A) CT scan (left) and photograph of slabbed core (right) showing identified types of fractures. Dh5-489 has naturally occurring geologic fractures (GF) and induced fractures: bedding-plane fracture (BPF) and slabbing fracture (SB). The 489.33 m sample was located along a GF. Removal of this point resulted in an uncertainty reduction of 10Ma B) Unrefined isochron from Dh5-489. C) Refined isochron. D) Trace element plots show abrupt changes in chemistry to identify chemical outliers (Triangles = Dh5. Squares = Dh2). Outliers were identified in Dh2 at 660.96 m (red circles) and Dh5 at 613.70 m (blue circles). Removal of the 660.96 m sample from the Dh2-660 isochron results in an uncertainty reduction of 11.7 Ma. E) Unrefined isochron of Dh2-660. F) Partially refined isochron from Dh2-660 with only 660.96 m removed.

samples can be caused by a variety of processes including localized fluid interaction, and/or detrital influences. Two chemical outliers are identified at Dh2-660.96 m and Dh5-613.70 m (Fig. 6D). The removal of a single chemical outlier in Dh2 at 660.96 m resulted in the reduction of uncertainty in age by 10.7 Ma (Fig. 6E and F). Unrefined and refined ages for all seven core segments including which samples were removed for refinement are in Table 2.

Re-Os ages from the Agardhfjellet Formation are a mix of Model 1 and Model 3 fits. Model 1 ages suggest that all of the uncertainty lies in the analytical uncertainties while Model 3 ages suggest geologic influences contribute to the uncertainty. Of the seven refined isochrons in the Agardhfjellet Formation, five have been identified as depositional ages (Dh2-660,674 and Dh5-489, 542, 658) and two have a high likelihood of over-printing or resetting because of diagenetic influences (Dh5-600 and Dh5-613). The five depositional isochrons place the Agardhfjellet Formation in the Middle Jurassic to earliest Cretaceous (Fig. 7, Table 2). Re-Os ages place the upper Oppdalen Member in the Oxfordian, the middle to upper Lardyfjellet Member in the Kimmeridgian, the lower Oppdalssåta Member and the middle Slottsmøya Member in the Volgian. The derived Osi from these isochrons show a steady increase in this ratio through the Middle to Late Jurassic and potential decrease in the early Cretaceous indicating shifting inputs or Re and Os in the ocean over this time. Although Dh5-600 and Dh5-613 have Early Cretaceous Re-Os ages, the biostratigraphy and the correlative section in Dh2 (674) both agree with a Kimmeridgian age (Table 2). The Model 1 ages from these Dh5 Lardyfjellet Member samples suggest that they show overprinting of the depositional ages events in the Early Cretaceous.

Including all samples, rhenium varied from 55.7 ppb to 3.6 ppb and osmium varied from 0.732 ppb to 0.206 ppb (Fig. 6D). There is somewhat limited spread in the  $^{187}\text{Re}/^{188}\text{Os}$  ratios

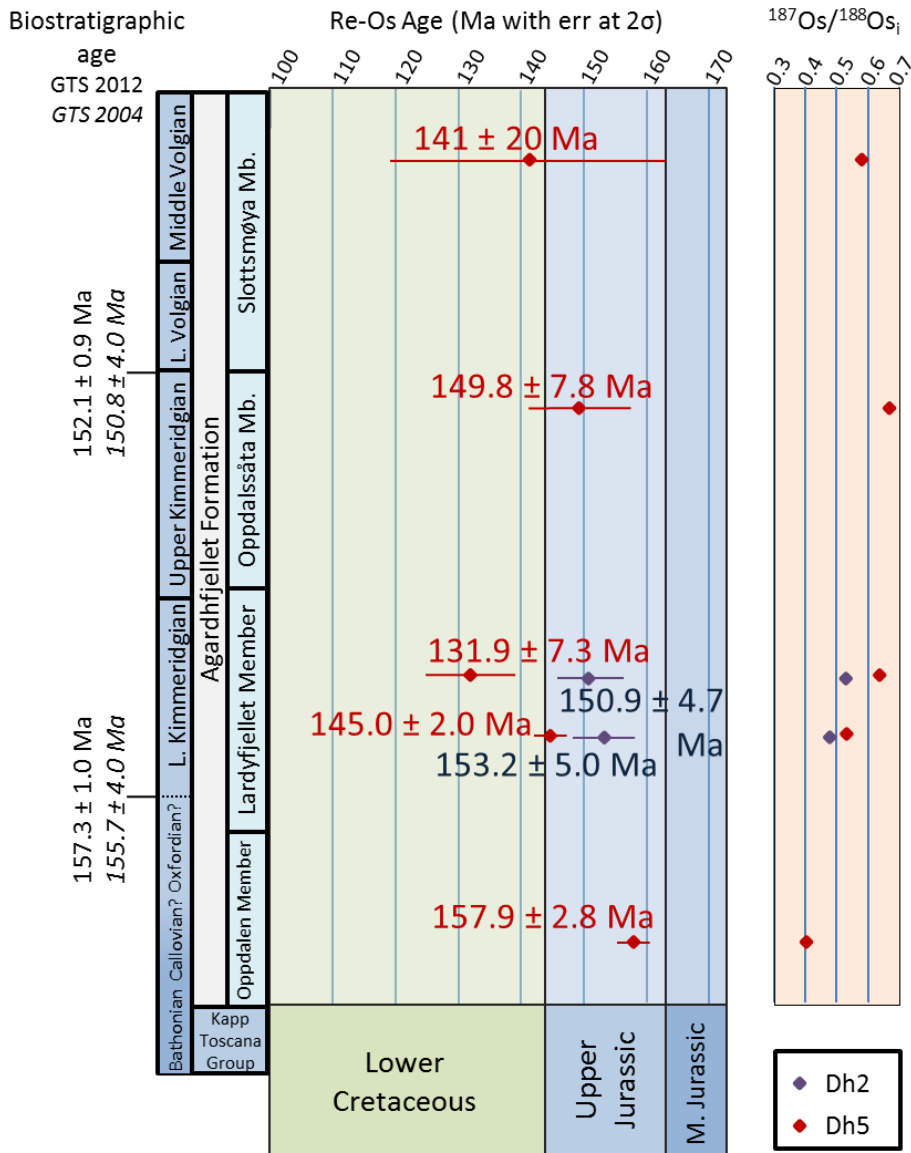


**Figure 7-Refined Re-Os ages with Os<sub>i</sub>.** Re-Os ages shown in comparison with biostratigraphic ages from GTS 2012 and GTS 2004 (italics). Os<sub>i</sub> derived from isochron regressions reported to right.

(616 to 119) and <sup>187</sup>Os/<sup>188</sup>Os ratios (2.2 to 0.637) across the Agardhfjellet Formation, negatively impacting the precision of the isochron.

### Rock Eval Results

The ORM of the Agardhfjellet Formation range in TOC from 1.19% to 11.7% (Fig. 8). A general decrease can be seen from the lower Lardyfjellet samples up into the Slottsmøya

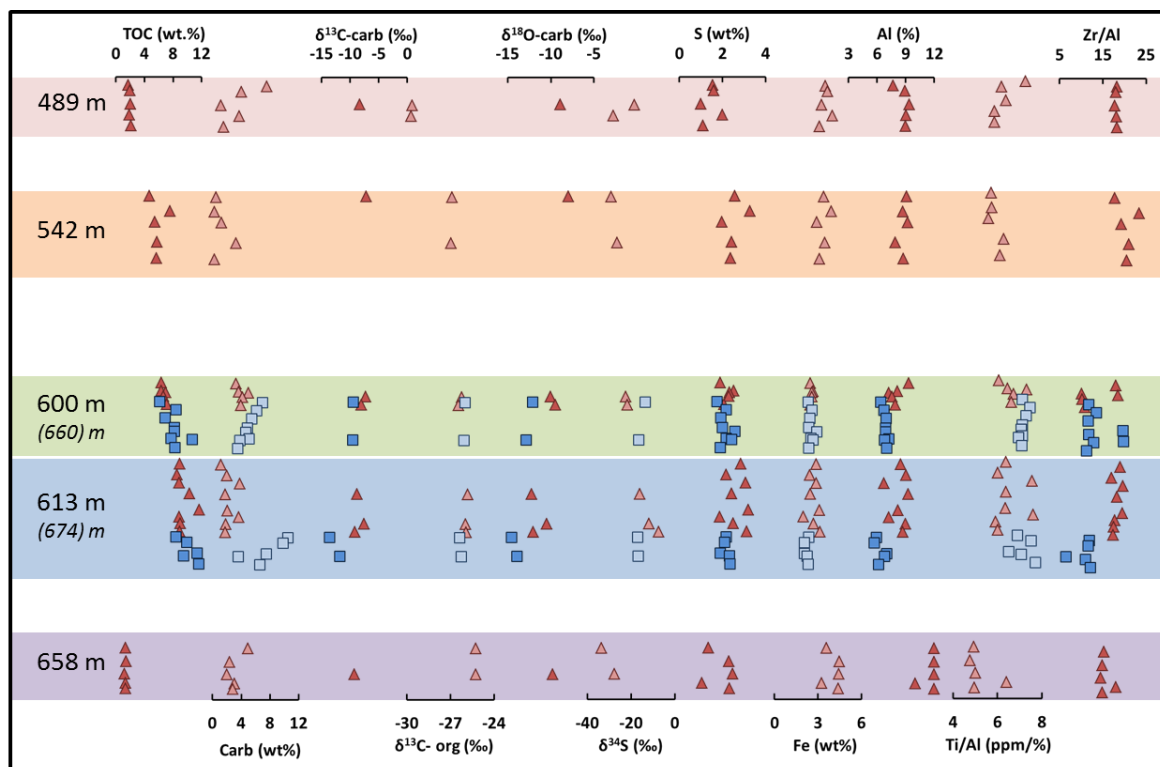


**Figure 8-Geochemical Plots with Depth.** Geochemical plots from the Agardhfjellet Formation. Percent carbonate is a calculated value from the Rock-Eval preparation process (see “External Chemical Analyses” for details). Triangles = Dh5. Squares = Dh2. Samples are listed in stratigraphic order. Core depths listed as Dh5 (Dh2). Trends are discussed in Results section of text.

samples. Intervals with the highest TOC are the Lardyfjellet Member samples ranging from 6.36% to 11.7% in Dh5 (600 and 613) and 6.11% to 11.7% in Dh2 (660 and 674). Low TOC intervals occur in the Slottsmøya and Oppdalen Members ranging from 1.77%-2.5% (Dh5-489) and 1.19% to 1.37% (Dh5-658) respectively. TOC in the Oppdalsåta Member ranged from 4.71 to 7.95% (Dh5-542). The hydrogen index (HI = mg HC/g TOC) and oxygen index (OI = mg  $\text{CO}_2/\text{g TOC}$ ) range from 31.3 to 126.5, and 2.4 to 23.1 respectively (Appendix A). Samples generally fall in the Type III kerogen field on the Kerogen Quality Plot indicating strong land-plant derived input to the organic matter (Fig. 9A). Samples from Dh5-658 fall just into Type IV kerogen (inertinite), although this may be a factor of high maturity as indicated by the Pseudo Van Krevelen Plot (Fig. 9B). Maturity proxies, including the production index (PI =

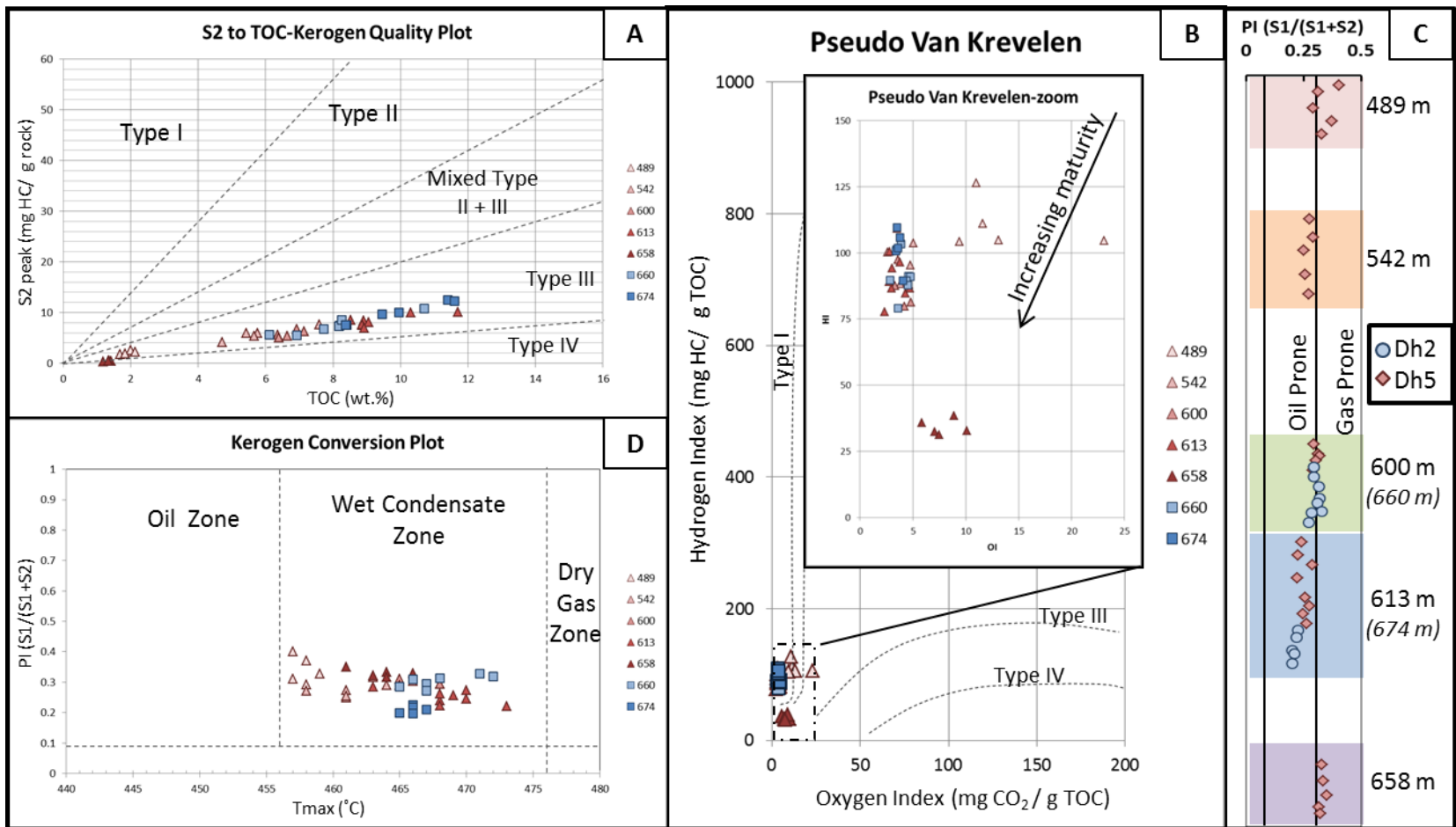


Figure 9-Rock-Eval Data Plots A) Agardhfjellet Formation plots within Type III kerogen indicating strong land-material influence. B) Agardhfjellet samples show high maturity. C) Production index shows high maturity in Dh5-489,542 and 658. Lardyfjellet Member samples (Dh2-660,674 and Dh5-600,613) show decreasing maturity with depth. See “Rock-Eval Results” for discussion. D) The Kerogen Conversion Plot shows all samples in the wet condensate field. Definitions of S1-S3 and  $T_{max}$  in “External Chemical Analysis” section.

S1/(S2+S1)), and Kerogen Conversion (PI vs TMax), indicate the Agardhfjellet Formation ranges from the late oil/condensate to gas prone window (Fig. 9C and, D). Maturity indicated by the production index does not directly follow a depth relationship. In fact, the relationship is generally inverse to depth through the Lardyfjellet Member section (Fig 9D). One explanation for this relationship could be the relatively short-term deep burial of the Agardhfjellet Formation. Burial below 1.5 km did not begin until ~65 Ma with the opening of the Greenland Sea. Although the Agardhfjellet Formation reached a depth of > 3 km, it was rapidly uplifted to ~1.5 km by 20 Ma and continued to uplift through the present-day (Mickleesen and Khorsani, 1991). Because of this relatively rapid burial and exhumation, samples with higher TOC, such as the Lardyfjellet Formation, may not have matured as fully as samples with low TOC, such as the Oppdalen and Slottsmøya Members.

### **Stable Isotope Results**

Stable isotopes of  $\delta^{13}\text{C}_{\text{org}}$ ,  $\delta^{13}\text{C}_{\text{carb}}$ ,  $\delta^{18}\text{O}_{\text{carb}}$ , and  $\delta^{34}\text{S}_{\text{V-CDT}}$  show several trends. Organic stable carbon ( $\delta^{13}\text{C}_{\text{org}}$ ) shows a decrease (Fig. 8) from the older Oppdalen Member (-25.25‰) to the younger Slottsmøya Member (-29.63‰). Inorganic carbon and oxygen are both highly negative and variable throughout the Agardhfjellet Formation (Fig. 8) indicating post-depositional influences. The  $\delta^{13}\text{C}_{\text{carb}}$  was lowest in Dh2-674 (-13.58‰ and -11.80‰) and the highest in Dh5-542 (-7.17‰). Similarly, the lowest values of  $\delta^{18}\text{O}_{\text{carb}}$  were also in Dh2-674 (-13.92‰ and -14.54‰) and highest in Dh5-542 (-7.99‰). The  $\delta^{34}\text{S}_{\text{V-CDT}}$  values are highly variable and ranged from -7.37‰ (Dh5-613) to -33.49‰ (Dh5-658). Generally lower  $\delta^{34}\text{S}_{\text{V-CDT}}$  values correlate with high pyrite content (Dh5-658) and higher  $\delta^{34}\text{S}_{\text{V-CDT}}$  correlate with higher wt.% TOC (Fig.8).

## Major and Trace Element Results

Major and trace element analyses show variability among the members of the Agardhfjellet Formation. Iron generally mirrors the sulfur content of samples. The highest concentrations of iron appear in samples with abundant visible pyrite and siderite (Dh5-658). Detrital proxies such as Al (wt.%) and Ti/Al (ppm/%) document variability in the general detrital input to Dh5-542, 600 and 613 as well as Dh2-674 (Fig. 8). Dh5-489 shows decreasing Al, increasing Ti relative to Al, and constant Zr/Al (ppm/%). This could be explained by a grain-size increase up-section. Dh5-658 shows consistency in all three proxies. The apparent outlier in Dh5-658 for Al-based proxies is a product of the way data over the detection limit were plotted (See Appendix A-Trace and Major Element for details).

Figure 10 shows selected redox-related proxies. The Agardhfjellet Formation is enriched in many chalcophilic and siderophilic element compared to average shale (Wedepohl, 1971) (Fig. 10A). Enrichment factors (EF) were calculated by normalizing Agardhfjellet samples to Al as a proxy for detrital influx and then dividing by Al-normalized average shale (i.e.  $(\text{Element}_{\text{AF}}/\text{Al}_{\text{AF}})/(\text{Element}_{\text{PAAS}}/\text{Al}_{\text{PAAS}})$ ). In general, redox sensitive elements such as U, V, and Mo show enrichment in the Lardyfjellet and Oppdalssåta Members, especially in Dh2-674, and depletion or average values in the Slottsmøya and Oppdalen Members. Most EF's range over an order of magnitude for the Agardhfjellet Formation; Co, however, is consistent and depleted ( $0.3 < \text{EF} < 0.6$ ) whereas Cd is highly variable and ranges from  $\text{EF} > 10$  to  $\text{EF} < 0.05$ . While redox sensitive elements are generally enriched compared to average shales, many are depleted when compared to average Late Jurassic to Early Cretaceous correlative Norwegian shales (Black line- Fig. 10A) (Lipinski et al., 2003; Markey et al., 2017-Fig 5). The exception is silver which is

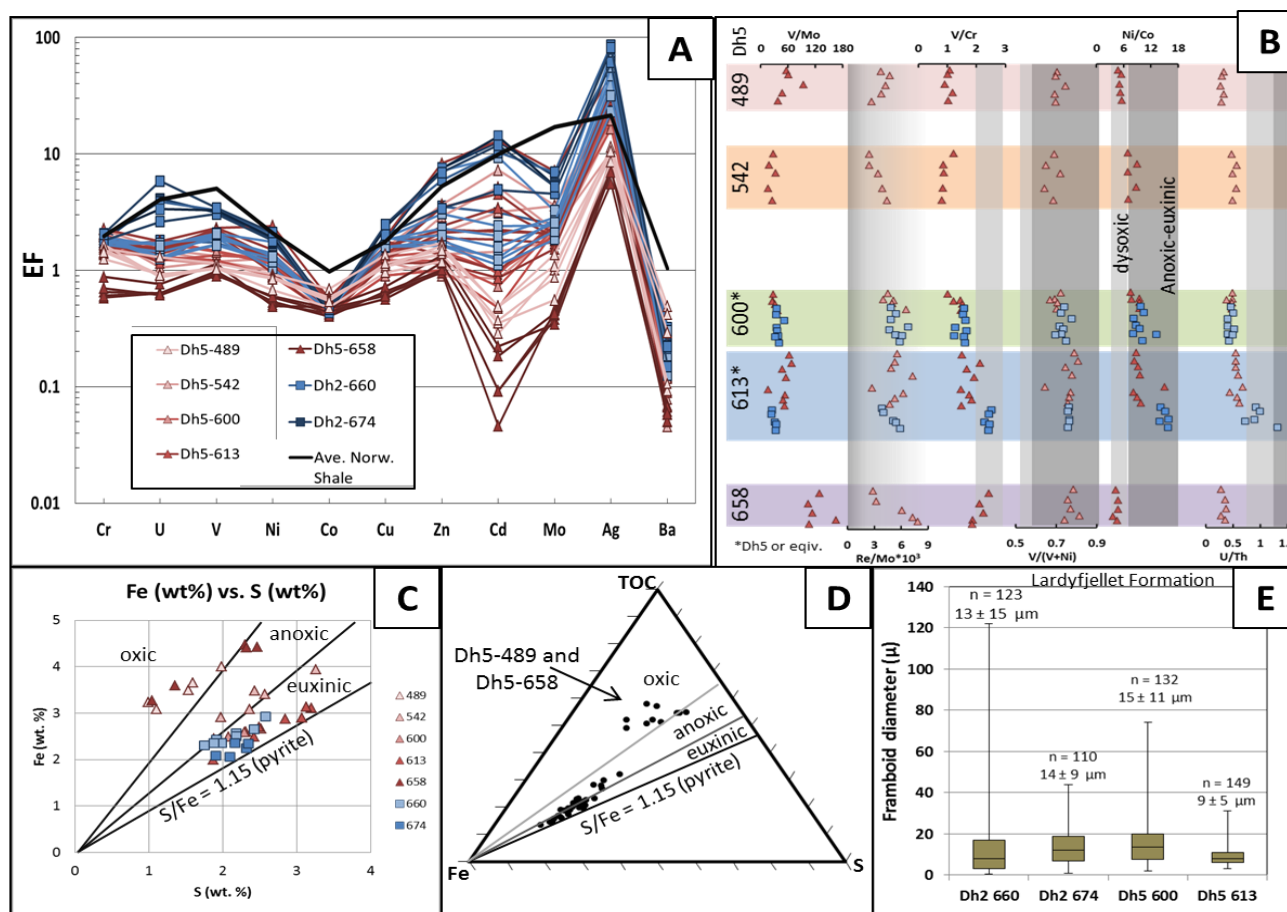


**Figure 10-Paleoredox Proxy Plots.** (see “Trace and major elements” for details). A) Enrichment factor (EF) for various trace elements of Agardhfjellet Formation in relation to average Norway (Wedepohl, 1971). The thick black line is an average for Norwegian, Late-Jurassic to Early Cretaceous black shales (Lipinski et al., 2003). B) Redox proxy ratios with depth. Light grey zones indicate values associated with dysoxic conditions. Dark grey is associated with anoxic to euxinic conditions. Triangles=Dh5, Squares=Dh2. C) Fe versus S concentration plot.  $S/Fe = 1.15$  is the pyrite line. D) Fe-S-TOC normalized concentration plot. The appearance of Dh5-489 and Dh5-658 in the oxic field of this plot and the previous plot is deceptive because Fe is included in non-sulfide phases. E) Framboid diameter data in the Lardyfjellet Member as box-and-whisker plots. Arithmetic means listed with sample size. All sections indicate anoxic to dysoxic conditions within the sediment column.

highly enriched compared to average shale, and enriched compared to Norwegian shale within the Lardyfjellet Member.

Chemical redox proxies for the Agardhfjellet Formation show variable results. The Fe versus S concentration plot and the Ni/Co proxy show two sections from the Agardhfjellet Formation have samples which fall into the oxic field (Dh5-489, 658) while the rest of the samples fit in the dysoxic to anoxic fields (Fig. 10B,C). Lines regressed through the samples of Dh5-489 and 658 on the Fe vs S plot show similar slopes to that of the pyrite line ( $S/Fe = 1.15$ ) with intercepts  $\sim 2.3$  wt.% Fe. This indicates that the degree of pyritization was high, but S was limiting; therefore, Fe was included in other phases such as high-Fe dolomite and/or siderite, both of which are abundant in the Agardhfjellet Formation. When normalized to TOC, Dh5-489 and 658 still fall into the oxic section (Fig. 10D). The higher V/Mo ratio in Dh5-658 also indicates that sulfate-reduction was not a dominant process and as such sulfur could be unavailable for pyrite formation (Fig. 10B). Two common redox proxies, U/Th and V/Cr, generally show core as oxic with a few dysoxic samples from Dh2-674, Dh5 613 and 658 (Fig. 10B). These proxies could be misleading as they are sensitive to additional parameters such as mineralogy, (i.e. U substitution in apatite which is a common mineral in Dh2-674) and provenance of sediments (i.e. Cr is higher in mafic sourced sediments and clays), (Tribovillard et al., 2006). Using the  $V/(V+Ni)$  proxy, all samples fit within the anoxic category (Fig. 10). Re/Mo has been used to define the degree of anoxia where low values are anoxic to euxinic and high values are suboxic to oxic (Crucius et al., 1996; Lipinski et al., 2003). Samples from the Agardhfjellet Formation show variable results in this metric as well. Cores from Dh5-658, 542 and Dh2-674 all show decreases in the Re/Mo ratio from suboxic to anoxic upsection, whereas the other samples are more scattered within these categories (Fig. 10B). Non-depositional ages

are associated with scatter in the Re/Mo ratios whereas depositional ages show steady trends in Re/Mo ratios.

## 5. DISCUSSION

### Ages

#### *Local stratigraphy*

Depositional ages indicate the Agardhfjellet Formation was deposited over at least 15 Ma from late Jurassic ( $157.9 \pm 2.9$  Ma) to early Cretaceous ( $141 \pm 20$  Ma). Ages are in general agreement with identified fossils. Two sections, the Slotsmoya (Dh5-489) and upper middle Lardyfjellet (Dh2-660), have slightly younger nominal ages, but are still within uncertainty of the expected ages (Table 2). A condensed section of  $\sim 7$  Ma in 12 m is recorded within the Oppdalen member between the upper Bathonian *Keplerites svalbardensis* and the late Oxfordian Re-Os age recorded from Dh5-658. This could contain one long or several shorter hiatuses in deposition, not unlike much of the Barents Sea where Middle Oxfordian strata are missing (Smelror et al., 2001). Changes in sea level from upper Bathonian to upper Oxfordian may have had a stronger effect on the Agardhfjellet Formation because of its near-shore setting, in contrast to the deeper shelf environment offshore.

Local alteration in the Lardyfjellet Formation at Dh5 is needed to account for the discrepancy of depositional ages in Dh2 and non-depositional ages in Dh5 (Fig. 7). Core from Dh5 shows more parting and structural fractures than Dh2. These could have provided easy conduits for fluid movement and disruption of the Re-Os system. Additionally the Dh5 core is less indurated than its equivalents in Dh2. The chemistry of redox sensitive elements and various proxies are much more scattered in Dh5 indicating post-depositional alteration (Fig. 8, 10). Cretaceous magmatic intrusions near Dh5 could have expelled or mobilized Re- and Os-bearing fluids that disturbed the Re-Os geochronometer. This could account for the Early Cretaceous ages

of the Lardyfjellet Member of Dh5. While no intrusive body was recorded in the Lardyfjellet Member at Dh5, several dolerite sills were identified from ~849-950 m in the adjacent Dh4 (Senger et al., 2014b). Nevertheless, the dolerite sills have low water contents, and spatially limited thermal areoles, so are not likely as a direct cause of disturbance.

#### *Bioturbation and Re-Os ages*

Surprisingly, one of the more robust ages comes from a heavily bioturbated sample, Dh5-658. Traditionally, bioturbation is interpreted as an indication of oxygenation of the sediment column. Churning alters redox conditions releasing sensitive metals such as Re and Os. In this case, the burrows have been mostly to fully pyritized and/or dolomitized and surrounded by siderite cement. Additionally, vertical burrows do not show compaction textures and horizontal burrows retain nearly equant cross-sections (Fig. 4E). This implies that the section was thoroughly cemented by siderite shortly after burial, preventing significant interaction of fluids with the Re-Os system. Therefore, the Dh5-658 age records a depositional age of Middle to Late Oxfordian despite heavy bioturbation.

#### *Regional comparisons*

Ages of the Lardyfjellet Member of the Agardhfjellet Formation at Longyearbyen show expected correspondence with ages of the Alge Member and middle to lower Krill Member of the Hekkingen Formation (Markey et al., 2017; Georgiev et al., 2017). Although relative uncertainties for Re-Os depositional ages for the Upper Jurassic are at least 0.4% and commonly >1% (including the  $^{187}\text{Re}$  decay constant uncertainty), the nominal ages within a stratigraphic sequence are remarkably consistent. This could indicate that reported age uncertainties may be over-estimated. However, there is more uncertainty in Agardhfjellet ages than in many of their counterparts in the Hekkingen Formation (Markey et al, 2017; Georgiev et al., 2017). Several

possibilities exist to explain these results. Samples with high uncertainties (Dh5-489, 542, and 600) were taken near gradations into coarser grained material. The covering sediments could have been affected by locally fluctuating oxygen conditions at the sediment-water interface during deposition which in turn affected fluid conditions in sediment pores below. Any oxidation and removal of Re and Os from the shales by related fluids would have to overcome the abundant organic matter in the Dh5 Lardyfjellet Member samples. As long as a reducing environment was maintained, the shales would rapidly sequester the Re and especially Os from the interacting fluids (Mahdaoui et al., 2015). Although this interaction may disturb the Os isotopic ratios, it also impact the Re/Os ratios proportionately (Hurtig et al., 2016). Thusly, the sediments lock in an early diagenetic age which is indistinguishable from the depositional age. Variation in the Os ratios on a sub-mm scale from this process could induce some scatter and therefor uncertainty in the reported ages. Another factor in the age uncertainties is the lack of spread in the  $^{187}\text{Re}/^{188}\text{Os}$  ratios relative to data collection uncertainties. While the Agardhfjellet Formation has a range of ~90-608 in the  $^{187}\text{Re}/^{188}\text{Os}$  ratio, individual cores have spreads of less than 50 (e.g., Dh5-600; 353-395) (Appendix C). By comparison, the  $^{187}\text{Re}/^{188}\text{Os}$  ratio in the Hekkingen Formation on the margin of the Hammerfest Basin ranges from 550 to 2250 (Markey et al., 2017).

The Agardhfjellet Formation at Longyearbyen has more in common with the Hekkingen Formation at Troms III (Finmark platform) than in Nordkapp or Hammerfest Basins (southern Barents Sea). Re-Os geochemistry of the Hekkingen Formation at Troms III has similar concentrations of Re and Os, as well as  $^{187}\text{Re}/^{188}\text{Re}$  ratios (Georgiev et al., 2017). When compared to the Nordkapp and Hammerfest Basins, the Agardhfjellet is relatively depleted in most redox elements including Re and Os (Markey et al., 2017; Georgiev et al., 2017).

Sedimentation rates for the Agardhfjellet Formation range from 8.7 m/My to 30.8 m/My. These are more similar to calculated depositional rates of the Hekkingen Formation at Troms III (16.8-13.1 m/My) than to the Hekkingen Formation at Nordkapp (1.3-5 m/My) or Hammerfest Basin (1.4-4.1 m/My) (Markey et al., 2017; Georgiev et al., 2016). The highest rate (30.8 m/My) is between the upper Lardyfjellet Member and the upper Oppdalssåta Member which includes several of regressive sequences with high clastic input. The paleogeography of the Troms III site was a proximal marine shelf environment, similar to the Agardhfjellet Formation, as opposed to the more distal Nordkapp and Hammerfest Basins.

#### *Implications for the Late Jurassic timescale*

Re-Os ages from the Oppdalssåta and Lardyfjellet Members at Longyearbyen are in better agreement with the defined boundaries of the Kimmeridgian from the 2004 Geologic Time Scale (GTS) than those of the 2012 GTS (Fig. 7). The Agardhfjellet Formation adds to a growing body of Late Jurassic radiometric ages including: (1) lower Kimmeridgian Re-Os results from the Kimmeridge Clay and Hekkingen Formation ( $154.1 \pm 2.2$  Ma; Selby, 2007:  $154.7 \pm 1.1$  Ma; Georgiev et al., 2017), and (2) an upper Oxfordian  $^{40}\text{Ar}$ - $^{39}\text{Ar}$  age from the Rosso Ammonitico Veronese Formation of Italy ( $156.1 \pm 0.89$  Ma; Pellenard et al., 2013). Combined, these recent radiometric ages suggest revisiting recommended ages for Late Jurassic stage boundaries, especially the Kimmeridgian-Oxfordian, which are currently calibrated by cyclostratigraphy and magnetostratigraphy.

#### **Anoxia and Restriction**

Sections of the Agardhfjellet Formation analyzed for this paper represent times of anoxic to dysoxic conditions. Many of the proxies used to indicate sediment and water column anoxia show oxic conditions; however, it is important to remember that these may be affected by

additional influences. Samples from the Oppdalen Members plot in the oxic section for many proxies traditionally used to characterize bottom water oxygenation. However, this core has delivered the Re-Os age with the least uncertainty. Pyritized burrows and siderite cement of the Oppdalen Member are better indications of anoxic conditions within the sediment column. Chemical parameters and framboid analyses from the upper Lardyfjellet Member indicate that sediment pore waters were generally anoxic/sulfidic to dysoxic (Fig. 10). A few thin (<1 mm) intervals of both Dh2 674 and Dh5 613 indicate a possible anoxic water column in addition to sediment anoxia, as the disseminated framboids have a diameter of less than 5  $\mu\text{m}$  (Fig. 10E). Partial to full pyritization of fossils also indicates anoxic sediment. Recrystallization of carbonate bioclasts into dolomite and high-Fe dolomite are additional indications of a persistently reducing environment in which methanogenesis is a dominant process. Post-depositional influences on the Lardyfjellet Member in Dh5 could have created the variability in redox sensitive elements and/or proxies.

### **Mid-Late Jurassic Climate Shift**

A decrease in  $\delta^{13}\text{C}_{\text{org}}$  and a corresponding increase in  $\text{Os}_i$  indicate a shifting climate over the late Jurassic. The decrease in  $\delta^{13}\text{C}_{\text{org}}$  from the Agardhfjellet Formation over the Late Jurassic agrees with both organic and inorganic  $\delta^{13}\text{C}$  trends observed by previous workers, not only in the Boreal realm (Koevoets et al., 2016; Markey et al., 2017), but throughout the globe (Weissert and Mohr, 1996; Weissert and Erba, 2004; Price et al., 2016). The trend has been interpreted by previous workers as a decrease in burial of organic material and increase in rainfall. The TOC of the Agardhfjellet Formation steadily decreases from the Lardyfjellet Member up through the Slottsmøya Member echoing these findings. Evidence for increased rainfall comes from the  $\text{Os}_i$

parameter. Increases in  $Os_i$  from the Agardhfjellet Formation correspond well with regional trends from several correlative formations (Fig. 11). This increase over the Middle to Late

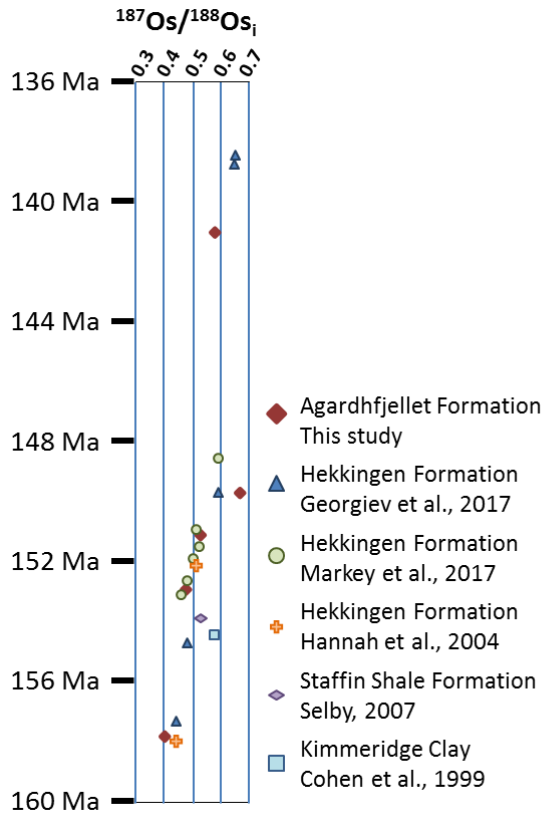


**Figure 11-Composite  $Os_i$  from Middle Jurassic to Early Cretaceous.**  $Os_i$  reported for this study are from calculated from depositional isochrons. Increasing  $Os_i$  throughout the Late Jurassic indicates increased continentally derived input into the oceans.

Jurassic is interpreted as increased continental weathering through this time. On their own, global events such as the development of the East Pacific Rise and spreading due to the breakup of Pangea cause a decrease in  $Os_i$  due to the increased mafic input to the oceanic systems. However, Cordilleran mountain building (e.g. Nevadan orogeny and Wrangelian arc volcanism) together with several collisional events along southern Eurasia, provide not only weathering potential but subduction related volcanic input contributing to the positive shift in  $Os_i$ . Coupling

$\delta^{13}\text{C}$  trends with  $\text{Os}_i$  trends indicate that the combination of changing climate and accelerated continental margin tectonism in the Late Jurassic lead to increased continental weathering.

## 6. CONCLUSION

Through systematically addressing non-isochroneity in the Re-Os system using detailed petrography, CT scans, and additional chemical data, it is possible to tease out useful information about black shales. Using this approach, we show that: (1) deposition of the Agardhfjellet Formation occurred throughout the Late Jurassic into the Early Cretaceous (157.9 Ma to 141 Ma with the *Amoeboceras subkitchini* zone lasting from at least 153.2 Ma to 150.9 Ma. (2) Throughout this time oceanic  $^{187}\text{Os}/^{188}\text{Os}$  ratios increased while  $\delta^{13}\text{C}_{\text{org}}$  decreased which is also seen globally. These trends indicate a shift in the Late Jurassic climate represented by an increase in continental weathering due to an increase in continental freeboard and/or an increase in rainfall. (3) Anoxic conditions during deposition of the Agardhfjellet Formation were not as persistent as several regional counterparts to the south: this most likely results from proximal shelf deposition with shifting oxygen minimum zones and intermittent sediment influx. Regionally, the Agardhfjellet Formation shares the most in common with the Hekkingen Formation at the Troms III locality which was also deposited on a marine shelf, with proximal sediment sources. Here we have used Re-Os geochronology to date a Late Jurassic formation, record temporal changes in anoxia within a basin, and infer changing climactic conditions and/or increased global tectonism by linking temporal trends in initial  $^{187}\text{Os}/^{188}\text{Os}$  ratios to continental weathering rates.

## REFERENCES

- Abbink, O., Targarona, J., Brinkhuis, H., Visscher, H., 2001. Late Jurassic to earliest Cretaceous palaeoclimatic evolution of the southern North Sea. *Global Planet. Change.* 20, 231-256. PII: S0921-8181(01)00101-1
- Algeo, T.J., Rowe, H., 2012. Paleoceanographic applications of trace-metal concentration data. *Chem. Geol.* 324-325, 6-18. doi:10.1016/j.chemgeo.2011.09.002
- Braathen A., Bergh., S.G. Maher Jr., H.D., 1999. Application of a critical edge taper model to the Tertiary transpressional fold-thrust belt on Spitsbergen, Svalbard. *Geol. Soc. Am. Bull.* 111(10), 1468-1485. doi: 10.1130/0016-7606(1999)111<1468:AOACWT>2.3.CO;2
- Braathen, A., Bælum, K., Christiansen, H.H., Dahl, T., Eiken, O., Elvebakk, H., Hansen, F., Hanssen, T.H., Jochmann, M., Johansen, T.A., Johnsen, H., Larsen, L., Lie, T., Mertes, J., Mørk, A., Mørk, M.B., Nemeč, W., Olaussen, S., Oye, V., Rød, K., Titlestad, G.O., Tveranger, J., Vagle, K., 2012. The Longyearbyen CO<sub>2</sub> Lab of Svalbard, Norway – initial assessment of the geological conditions for CO<sub>2</sub> sequestration. *Norw. J. Geol.* 92, 353-376.
- Cohen, A.S., Coe, A.L., Bartlett J.M., Hawkesworth, C.J., 1999. Precise Re-Os ages of organic-rich mudrocks and the Os isotope composition of Jurassic seawater. *Earth Planet. Sci. Lett.* 167(3-4), 159-173.
- Cohen, A.S., 2004. The rhenium-osmium isotope system: applications to geochronological and paleoenvironmental problems. *J. Geol. Soc, London.* 161, 729-734.
- Cope, J.C.W., 2008. Drawing the line: the history of the Jurassic-Cretaceous boundary. *Proceedings of the Geologists Association.* 119(1), 105-117.
- Creaser R.A., Sannigrahi, P., Chacko, T., Selby, D., 2002. Further evaluation of the Re-Os geochronometer in organic-rich sedimentary rocks: A test of hydrocarbon maturation effects in the Exshaw Formation, Western Canada Sedimentary Basin. *Geochim. Cosmochim. Acta.* 66(19), 3441-3452. PII S0016-7037(02)00939-0
- Crucius, J., Calvert, S., Pedersen, T., Sage, D., 1996. Rhenium and molybdenum enrichments in sediments as indicators of oxic, suboxic and sulfidic conditions of deposition. *Earth Planet. Sci. Lett.* 145, 65-78.
- Ditchfield, P.W., 1997. High northern palaeoaltitude Jurassic-Cretaceous palaeotemperature variation: new data from Kong Karls Land, Svalbard. *Palaeogeogr. Palaeoclimatol. Palaeoecol.* 130, 163-175. PH S0031-0182(96)00054-5

- Dypvik, H., 1985. Jurassic and Cretaceous Black Shales of the Janusfjellet Formation, Svalbard, Norway. *Sediment. Geol.* 41, 235-248.
- Dypvik, H., Nagy, J., Eikeland, T.A., Backer-Owe, K., Andresen, A., Haremo, P., Bjærke, T., Johansen, H., Elverhøi, A., 1991. The Janusfjellet subgroup (Bathonian to Hauterivian) on central Spitsbergen—a revised lithostratigraphy. *Polar Res.* 9, 21–43.
- Dypvik, H., Håkansson, E., Heinberg, C., 2002. Jurassic and Cretaceous palaeogeography and stratigraphic comparisons in the North Greenland-Svalbard Region. *Polar Res.*, 21(1), 91-108.
- Finlay, A.J., Selby, D., Gröcke, D.R., 2010. Tracking the Hirnantian glaciation using Os isotopes. *Earth Planet. Sci. Lett.* 293, 339-348. doi:10.1016/j.epsl.2010.02.049
- Georgiev S., Stein, H.J., Hannah, J.L., Bingen, M., Weiss, H.M., Piasecki, S., 2011. Hot acidic Late Permian seas stifled life in record time. *Earth Planet. Sci. Lett.* 310(3-4), 389-400.
- Georgiev S., Stein, H.J., Hannah, J.L., Weiss, H.M., Bingen, B., Xu, G., Rein, E., Hatløy, V., Løseth, H., Nali, M., Piasecki, S., 2012. Chemical signals for oxidative weathering predict Re-Os isochroneity in black shales, East Greenland. *Chem. Geol.* 324-325, 108-121. doi:10.1016/j.chemgeo.2012.01.003
- Georgiev, S.V., Stein, H.J., Hannah, J.L., Henderson, C.M., Algeo, T.J., 2015. Enhanced recycling of organic matter and Os-Isotopic evidence for multiple magmatic or meteoric inputs to the Late Permian Panthalassic Ocean, Opal Creek, Canada. *Geochim. Cosmochim. Acta.* 150, 192-210. <http://dx.doi.org/10.1016/j.gca.2014.11.019>
- Georgiev S.V., Stein, H.J., Hannah, J.L., Xu, G., Bingen, B., Weiss, H.M., 2017. Timing, duration, and causes for Late Jurassic-Early Cretaceous anoxia in the Barents Sea. *Earth Planet. Sci. Lett.* 461(1), 151-162. <http://dx.doi.org/10.1029/2009GC002788>
- Gradstein F.M., Ogg, J.G., Schmitz, M., Ogg, G. (Eds.) 2012. *The Geologic Time Scale 2012* two-volume set. Elsevier, Oxford. 731-779.
- Gröcke D.R., Price, G.D., Ruffell, A.H., Mutterlose, J., Baraboshkin, E., 2003. Isotopic evidence for Late Jurassic-Early Triassic climate change. *Palaeogeogr. Palaeoclimatol. Palaeoecol.* 202, 97-118. doi:10.1016/S0031-0182(03)00631-X
- Hannah, J.L., Georgiev, S., Xu, G., Stein, H.J., 2012. A global Os isotope signal in a narrow seaway – the Late Jurassic from the Barents Sea to S. England. *Mineralogical Magazine.* 76, 1807.
- Hammer, Ø., Collignon, M., Nakrem, H.A., 2012. Organic carbon isotope chemostratigraphy and cyclostratigraphy in the Volgian of Svalbard. *Norw. J. Geol.* 92, 103-112.

- Hammer, Ø., 2014. Initial stratigraphic columns and biostratigraphy for DH2 and DH5R, Adventdalen. written communication.
- Heumann, K., 1988. Isotope dilution mass spectrometry. In: Adams, F., Gijbels, R., Van Greiken, R. (Eds.), *Inorganic Mass Spectrometry*. Wiley Interscience, New York. pp. 301–376.
- Hurtig, N.C., Stein, H.J., Hannah, J.L., 2016. Re-Os systematics at the water-oil interface from an experimental perspective. *Geol. Soc. America Abstracts with Programs* 48:7, doi: 10.1130/abs/2016AM-283562
- Kendall B., Creaser, R.A., Gordon, G.W., Anbar, A.D., 2009. Re-Os and Mo isotope systematics of black shales from the Middle Proterozoic Velkerri and Wollgorang Formations, McArthur Basin, northern Australia. *Geochim. Cosmochim. Acta.* 73, 2534-2558. doi:10.1016/j.gca.2009.02.013
- Koevoets M.J., Abay, T.B., Hammer, Ø., Olausen, S., 2016. High-resolution organic carbon-isotope stratigraphy of the Middle Jurassic-Lower Cretaceous Agardhfjellet Formation of central Spitsbergen, Svalbard. *Paleogeogr. Palaeoclimatol. Palaeoecol.* 449, 266-274. <http://dx.doi.org/10.1016/j.palaeo.2016.02.029>
- Krajewski, K. P., 2004. Carbon and oxygen isotopic survey of diagenetic carbonate deposits in the Agardhfjellet Formation (Upper Jurassic), Spitsbergen: preliminary results. *Pol. Polar Res.* 25(1), 27-43.
- Lazar, O.R., Bohacs, K.M., Schieber, J., Macquaker, J.H.S., and Demko, T.M., 2015. Mudstone Primer: Lithofacies variations, diagnostic criteria, and sedimentologic-stratigraphic implications at lamina to bedset scales. *SEPM Concepts in Sedimentology and Paleontology* 12, 198
- Lipinski, M., Warning, B., Brumsack, H-J., 2003. Trace metal signatures of Jurassic/Cretaceous black shales from the Norwegian Shelf and Barents Sea. *Paleogeogr. Palaeoclimatol. Palaeoecol.* 190, 459-475. PII:S0031-0182(02)00619–3
- Ludwig, K.R., 2012, *Isoplot/Ex Version 3.75, A Geochronological Toolkit for Microsoft Excel*. Berkeley Geochronol. Cent. Spec. Publ. 5, 75.
- Markey R., Stein, H.J., Hannah, J.L., Georgiev, S.V., Pedersen, J.H., Dons, C.E., 2017. Re-Os identification of glide faulting and precise ages for correlation from the Upper Jurassic Hekkingen Formation, southwestern Barents Sea. *Paleogeogr. Palaeoclimatol. Palaeoecol.* 466, 209-220. doi:10.1016/j.palaeo.2016.11.032
- Michelsen, J.K., Khorasani, G.K., 1991. A regional study on coals from Svalbard: organic facies, maturity and thermal history. *Bull. Soc. Geol. France.* 162(2), 385-397.

- Mahdaoui F., Michels, R., Reisberg, L., Puojol, M., Poirier, Y., 2015. Behavior of Re and Os during contact between an aqueous solution and oil: Consequences for the application of the Re-Os geochronometer to petroleum. *Geochim. Cosmochim. Acta.* 158, 1-21. doi:10.1016/j.gca.2015.02.009
- Marshall, C., Ugunna, J., Large, D.J., Meredith, W., Jochmann, M., Friis, B., Vane, C., Spiro, B.F., Snape, C.E., Orheim, A., 2015. Geochemistry and petrology of Paleocene coals from Spitzbergen – Part 2: Maturity variations and implications for local and regional burial models. *Int. J. Coal. Geol.* 143, 1-10. doi:10.1016/j.coal.2015.03.013
- Mørk, A., Dallmann, W.K., Dypvik, H., Johannessen, E.P., Larssen, G.B., Nagy, J., Nøttvedt, A., Olausen, S., Pčhelina, T.M., Worsley, D., 1999 Mesozoic lithostratigraphy. In: Dallmann, W.K., (Ed.), *Lithostratigraphic lexicon of Svalbard Review and Reconstructions for Nomenclature Use. Upper Palaeozoic to Quaternary Bedrock.* Norsk Polarinstitutt Tromsø, Norway. 127-214.
- Nagy J., Løfaldli, M., Bäckström, S.A., 1988. Aspects of foraminiferal distribution and depositional conditions in the middle Jurassic to early cretaceous shales in eastern Spitsbergen. *Abh. Geol. Bund.* 30, 287-300.
- Nagy, J., Basov, V.A., 1989. Revised foraminiferal taxa and biostratigraphy of Bathonian to Rhyazanian deposits in Spitsbergen. *Micropaleontology.* 44(3), 217-255.
- Page, K.N., 2008. The evolution and geography of Jurassic ammonoids. *Proceedings of the Geologist's Association.* 119(1), 35-57.
- Pellenard, P., Nomade, S., Martire, L., De Oliveira Ramalho, F., Monna, F., Guillou, H., 2013. The first  $^{40}\text{Ar}$ - $^{39}\text{Ar}$  date from Oxfordian ammonite-calibrated volcanic layers (bentonites) as a tie-point for the Late Jurassic. *Geol. Mag.* 150(06), 1136-1142.
- Price, G.D., Fözy, I., Pálffy, J., 2016. Carbon cycle history through the Jurassic-Cretaceous boundary: A new global  $\delta^{13}\text{C}$  stack. *Paleogeogr. Palaeoclimatol. Palaeoecol.* 451, 46-61. doi:10.1016/j.palaeo.2016.03.016
- Ravizza, G., Norris, R.N., Blusztajn, J., 2001. An osmium isotope excursion associated with the late thermal maximum: Evidence of intensified chemical weathering. *Paleoceanography.* 16(2), 155-163.
- Ravizza, G., Turekian, K.K., 1989. Application of the  $^{187}\text{Re}$ - $^{187}\text{Os}$  system to black shale geochemistry. *Geochim. Cosmochim. Acta.* 53, 3257-3262.
- Rooney, A.D., Selby, D., Houzay, J-P., Renne, P.R., 2010. Re-Os geochronology of a Mesoproterozoic sedimentary succession, Taoudeni basin, Mauritania: Implications for

- basin-side correlations and Re-Os organic rich sediments systematics. *Earth Planet. Sc. Lett.* 289, 486-496. doi:10.1016/j.epsl.2009.11.039
- Selby, D., 2007. Direct Rhenium-Osmium age of the Oxfordian Kimmeridgian boundary, Staffin Bay, Isle of Skye, UK., and the Late Jurassic time scale. *Norw. J. Geol.* 87(3), 291-299.
- Selby, D., Creaser, R.A., 2003a. Re-Os geochronology of organic rich sediments: an evaluation of organic matter analysis methods. *Chem. Geol.* 200, 225-240. doi:10.1016/S0009-2541(03)00199-2
- Selby, D., Creaser, R.A., 2003b. Direct Radiometric dating of the Devonian-Mississippian time-scale boundary using the Re-Os black shale geochronometer. *Geology.* 33(7), 545-548. doi: 10.1130/G21324.1
- Senger, K., Tveranger, J., Ogata, K., Braathen, A., Planke, S., 2014a. Late Mesozoic magmatism in Svalbard: A Review. *Earth-Sci. Rev.* 130, 121-144. doi:10.1016/j.earscirev.2014.09.002
- Senger K., Planke, S., Polteau, S. Ogata, K., Svensen, H., 2014b. Sill emplacement and contact metamorphism in a siliciclastic reservoir on Svalbard, Arctic Norway. *Norw. J. Geol.* 94, 155-169.
- Smelror M., Mørk, A., Mørk, M.B.E., Weiss, H.M., Løseth, H., 2001. Middle Jurassic-Lower Cretaceous transgressive-regressive sequences and facies distribution off northern Nordland and Troms, Norway. *Norwegian Petroleum Society Special Publications* 10, 211-232.
- Torsvik, T.H., Carlos, D., Mosar, J., Cocks, L.R.M., Maime, T. 2002. Global reconstructions and North Atlantic paleogeography 440 Ma to recent. In: Eide, E.A. (Ed.) *BATLAS – Mid Norway Plate Reconstruction Atlas with Global and Atlantic Perspectives*. Geological Survey of Norway, Trondheim, pp. 18-39
- Tribovillard, N., Algeo, T.J., Lyons, T., Riboulleau, A., 2006. Trace metals as paleoredox and paleoproductivity proxies: An update. *Chem. Geol.* 232(1). 12-32. doi:10.1016/j.chemgeo.2006.02.012
- Turgeon, S.C., Creaser, R.A., 2008. Cretaceous oceanic anoxic event 2 triggered by a massive magmatic episode. *Nature.* 454, 323-326. doi:10.1038/nature07076
- Wedepohl, K.H., 1971. Environmental influences on the chemical composition of shales and clays. In: Ahrens, L.H., Press, F., Runcorn, S.K., Urey, H.C., (Eds.) *Physics and Chemistry of the Earth*. Pergamon. Oxford. 305-333.
- Weissert, H., Mohr, H., 1996. Late Jurassic climate and its impact on carbon cycling. *Paleogeogr. Palaeoclimatol. Palaeoecol.* 122, 27-43.

- Weissert, H., Erba, E.B., 2004. Volcanism, CO<sub>2</sub> and palaeoclimate: a Late Jurassic-Early Cretaceous carbon and oxygen isotope record. *J. Geol. Soc. London.* 161, 695-702.
- Wierzbowski, A., Hryniewicz, K., Hammer, Ø., Nakrem, H.A., Little, C.T.S., 2011. Ammonites from hydrocarbon seep carbonate bodies from the uppermost Jurassic – lowermost Cretaceous of Spitsbergen and their biostratigraphical importance. *N. Jb. Geol. Paläont. Abh.* 262(3), 267-288.
- Xu, G., Hannah, J.L., Stein, H.J., Bingen, B., Yang, G., Zimmerman, A., Weitschat, W., Mørk, A., Weiss, H.M., 2009. Re-Os geochronology of Arctic black shales to evaluate the Anisian-Ladinian boundary and global faunal correlations. *Earth Planet. Sc. Lett.* 288, 581-587. doi:10.1016/j.epsl.2009.10.022
- Xu, G., Hannah, J.L., Stein, H.J., Mørk, A., Vigran, J.O., Bingen, B., Schutt, D.L., Lundschie, B.A., 2014. Cause of Upper Triassic climate crisis revealed by Re-Os geochemistry of Boreal black shales. *Paleogeogr. Palaeoclimatol. Palaeoecol.* 395, 222-232. doi:10.1016/j.palaeo.2013.12.02
- Yang, G., Hannah, J.L., Zimmerman, A., Stein, H.J., Bekker, A., 2009. Re-Os depositional age for Archean carbonaceous slates from the southwestern Superior Province: Challenges and insights. *Earth Planet. Sci. Lett.* 280, 83-92.

APPENDIX A

Table 3-Geochemical Data

		Re-Os Geochemistry: AIRE®													Re Blank			Os Blank		
Sample Depth	Drill Hole	AIRIE											Blank			Contribution				
		RUN #	Re (ppb)	Err (2-s)	Re % Error	Os (ppb)	Os err (2-s)	Os % Error	187Re/188Os	err (2-s)	187Os/188Os	err (2-s)	rho	ID	%	%				
489.33	Dh5	ORG-1868	8.5904	0.0832	0.9683	0.3071	0.0002	0.0741	148.3309	1.9784	0.8972	0.0019	0.0744	I	1.5%	0.1%				
489.355	Dh5	ORG-1477	10.6884	0.0181	0.1693	0.3170	0.0002	0.0493	181.1404	0.4364	1.0094	0.0014	0.2551	B	0.2%	0.2%				
489.4	Dh5	ORG-1429	6.5087	0.1322	2.0318	0.2782	0.0002	0.0542	123.6351	3.4461	0.8681	0.0014	0.0247	A	0.3%	0.3%				
		ORG-1476	6.3560	0.0103	0.1621	0.2808	0.0001	0.0534	119.5181	0.2810	0.8625	0.0013	0.2908	B	0.3%	0.2%				
489.44	Dh5	ORG-1478	11.1321	0.0199	0.1787	0.3057	0.0002	0.0808	196.4010	0.5533	1.0403	0.0023	0.3772	B	0.2%	0.2%				
489.48	Dh5	ORG-1548	9.7970	0.0944	0.9639	0.3177	0.0005	0.1419	164.8318	2.2209	0.9624	0.0040	0.1306	D	1.2%	0.2%				
		ORG-1479	9.8058	0.0192	0.1961	0.3268	0.0002	0.0653	159.8886	0.4617	0.9390	0.0017	0.2928	B	0.2%	0.2%				
542.21	Dh5	ORG-1531	14.3716	0.1357	0.9445	0.2664	0.0003	0.1154	303.2129	3.9750	1.4136	0.0045	0.1099	C	0.8%	0.1%				
542.265	Dh5	ORG-1532	22.6133	0.2123	0.9389	0.3438	0.0003	0.0823	379.0687	4.9069	1.6297	0.0036	0.0790	C	0.5%	0.1%				
542.305	Dh5	ORG-1430	16.7229	0.0582	0.3482	0.2594	0.0002	0.0852	369.8322	1.8352	1.5894	0.0037	0.1950	A	0.1%	0.3%				
		ORG-1533	16.5213	0.1555	0.9414	0.2570	0.0002	0.0813	369.0497	4.7895	1.5963	0.0035	0.0791	C	0.7%	0.1%				
542.38	Dh5	ORG-1534	32.6589	0.3099	0.9488	0.3282	0.0004	0.1143	607.6832	7.9837	2.1771	0.0062	0.1008	C	0.4%	0.1%				
542.44	Dh5	ORG-1535	25.5300	0.2377	0.9310	0.2855	0.0002	0.0810	536.9123	6.8867	2.0128	0.0042	0.0742	C	0.5%	0.1%				
600.32	Dh5	ORG-1431	26.8950	0.0868	0.3227	0.3890	0.0002	0.0538	393.3956	1.7621	1.5140	0.0022	0.1420	A	0.0%	0.1%				
		ORG-1672	26.9579	0.0605	0.2246	0.3882	0.0005	0.1271	394.7015	1.5390	1.5064	0.0047	0.5095	F	0.0%	0.2%				
600.35	Dh5	ORG-1673	24.1325	0.0622	0.2576	0.3846	0.0005	0.1231	353.1076	1.5003	1.4132	0.0041	0.4891	F	0.7%	0.2%				
600.355	Dh5	ORG-1869	28.7533	0.1698	0.5906	0.4183	0.0004	0.0940	390.2427	3.2208	1.4924	0.0038	0.1420	I	0.5%	0.2%				
600.37	Dh5	ORG-1674	25.6274	0.0682	0.2663	0.3908	0.0004	0.1135	370.8103	1.5771	1.4576	0.0038	0.4689	F	0.6%	0.1%				
600.4	Dh5	ORG-1675	30.6349	0.0680	0.2219	0.4519	0.0006	0.1275	384.2806	1.4876	1.4823	0.0047	0.5096	F	0.5%	0.1%				
613.53	Dh5	ORG-1571	23.5202	0.0609	0.2588	0.4274	0.0003	0.0675	304.4095	1.1260	1.2613	0.0025	0.2144	E	0.8%	0.2%				
613.57	Dh5	ORG-1570	21.5638	0.0506	0.2344	0.3983	0.0002	0.0535	299.0338	0.9855	1.2491	0.0019	0.1971	E	0.9%	0.2%				
613.6	Dh5	ORG-1870	23.3720	0.1541	0.6595	0.4503	0.0003	0.0697	285.3726	2.6007	1.2080	0.0024	0.0972	I	0.7%	0.1%				
613.64	Dh5	ORG-1569	39.9857	0.0915	0.2288	0.5361	0.0004	0.0688	425.8954	1.4048	1.5543	0.0030	0.2377	E	0.5%	0.1%				
613.7	Dh5	ORG-1432	47.1492	0.1117	0.2369	0.6973	0.0005	0.0665	380.7747	1.2983	1.4202	0.0026	0.2506	A	0.0%	0.1%				
		ORG-1568	47.1507	0.1030	0.2184	0.7257	0.0007	0.0899	363.3837	1.2184	1.3620	0.0034	0.3232	E	0.4%	0.1%				
613.725	Dh5	ORG-1871	27.5545	0.1734	0.6292	0.4596	0.0003	0.0634	334.2852	2.9026	1.3323	0.0023	0.2335	I	0.6%	0.1%				
613.75	Dh5	ORG-1567	28.6529	0.2625	0.9163	0.5002	0.0003	0.0681	317.8705	4.0080	1.2866	0.0025	0.0635	E	0.7%	0.1%				
613.78	Dh5	ORG-1566	23.4449	0.0679	0.2895	0.4936	0.0002	0.0402	258.8822	1.0310	1.1353	0.0013	0.1190	E	0.8%	0.1%				
658.01	Dh5	ORG-1537	3.8219	0.0251	0.6555	0.2060	0.0001	0.0462	95.2574	0.8580	0.6386	0.0009	0.0625	C	4.9%	0.2%				
		ORG-1549	3.6230	0.0367	1.0129	0.2070	0.0001	0.0486	89.9604	1.2509	0.6370	0.0009	0.0446	D	3.3%	0.3%				
658.06	Dh5	ORG-1550	5.1853	0.0540	1.0420	0.2192	0.0002	0.0730	122.9708	1.7636	0.7301	0.0016	0.0626	D	2.3%	0.3%				
658.105	Dh5	ORG-1551	8.9197	0.0859	0.9630	0.2273	0.0002	0.1094	209.3330	2.7948	0.9470	0.0031	0.0997	D	1.4%	0.3%				
658.14	Dh5	ORG-1552	7.3772	0.0723	0.9800	0.2076	0.0003	0.1518	188.1462	2.5826	0.8977	0.0041	0.1324	D	1.6%	0.3%				
658.16	Dh5	ORG-1536	11.7667	0.3027	2.5728	0.2438	0.0015	0.6227	262.2748	9.7696	1.1062	0.0188	0.2268	C	1.6%	0.1%				
		ORG-1553	11.6593	0.1097	0.9412	0.2520	0.0008	0.3243	250.0218	3.5795	1.0636	0.0095	0.3047	D	1.0%	0.3%				
660.82	Dh2	ORG-1762	22.6044	0.0489	0.2161	0.2911	0.0002	0.0635	448.6483	1.3926	1.6582	0.0028	0.2501	H	0.6%	0.2%				
660.85	Dh2	ORG-1676	30.3977	0.0706	0.2324	0.4001	0.0007	0.1830	437.8051	2.0408	1.6272	0.0075	0.5583	F	0.5%	0.1%				
		ORG-1763	30.1960	0.0693	0.2295	0.4010	0.0003	0.0868	433.4523	1.4979	1.6199	0.0037	0.3128	H	0.4%	0.1%				
660.88	Dh2	ORG-1764	18.1800	0.0412	0.2266	0.3025	0.0002	0.0641	336.7195	1.0980	1.3762	0.0024	0.2546	H	0.7%	0.2%				
660.915	Dh2	ORG-1872	33.0557	0.1973	0.5970	0.4159	0.0003	0.0647	460.0972	3.7921	1.6700	0.0029	0.0976	I	0.5%	0.1%				
660.93	Dh2	ORG-1765	26.1448	0.0573	0.2191	0.4022	0.0002	0.0607	367.2610	1.1524	1.4488	0.0024	0.2494	H	0.5%	0.1%				
660.955	Dh2	ORG-1873	24.7190	0.1541	0.6232	0.3616	0.0003	0.0870	388.1518	3.3646	1.4957	0.0035	0.1251	I	0.7%	0.1%				
660.96	Dh2	ORG-1766	39.1507	0.0946	0.2416	0.5511	0.0003	0.0635	407.3662	1.4043	1.5823	0.0027	0.2372	H	0.3%	0.1%				
660.99	Dh2	ORG-1767	30.8128	0.0661	0.2145	0.4198	0.0003	0.0631	420.8036	1.2999	1.5824	0.0026	0.2615	H	0.4%	0.1%				
674.08	Dh2	ORG-1707	42.9179	0.0929	0.2164	0.4908	0.0007	0.1425	512.5796	1.9655	1.7843	0.0067	0.4399	G	0.5%	0.1%				
674.1	Dh2	ORG-1708	46.5710	0.0978	0.2100	0.6003	0.0006	0.1052	445.9186	1.5103	1.6082	0.0045	0.3802	G	0.4%	0.1%				
674.14	Dh2	ORG-1677	55.7373	0.1295	0.2324	0.6972	0.0008	0.1081	461.5587	1.7269	1.6457	0.0044	0.4299	F	0.3%	0.1%				
		ORG-1709	55.5263	0.1185	0.2134	0.6975	0.0007	0.1000	459.6283	1.5543	1.6477	0.0044	0.3726	G	0.4%	0.1%				
674.15	Dh2	ORG-1710	48.9825	0.1084	0.2212	0.5896	0.0005	0.0778	482.6734	1.5773	1.7056	0.0035	0.2864	G	0.4%	0.1%				
674.18	Dh2	ORG-1711	55.5162	0.1158	0.2087	0.7320	0.0006	0.0777	435.0198	1.3557	1.5872	0.0033	0.3043	G	0.4%	0.1%				

Errors for Re and Os data are 2-sigma. Rho is the error correlation between 187Re/188Os and 187Os/188Os. All data are blank corrected using total analytical blanks (TABs).

\* Italics indicate a sample used to determine the proper amount of spiking solution to add in accordance with ideal ratios for isotope dilution spectrometry (See Heumann).

Table 3 cont.		Rock-Eval: Geomark											Production Index SI/(SI+S2)	Experimental Notations
Sample Depth	Drill Hole	Percent Carbonate (wt%)	Leco TOC (wt%)	Rock-Eval-2 S1 (mg HC/g)	Rock-Eval-2 S2 (mg HC/g)	Rock-Eval-2 S3 (mg CO2/g)	Rock-Eval-2 Tmax (°C)	Calculated %Ro (RETMAX)	Hydrogen Index (S2x100/TOC)	Oxygen Index (S3x100/TOC)	S2/S3 Conc. (mg HC/mg CO2)	SI/TOC Norm. Oil Content		
489.33	Dh5	7.518796992	1.69	1.187	1.77	0.39	457	1.066	104.7337278	23.07692308	4.538461538	70.23668639	0.4014204	Low Temp S2 Shoulder
489.355	Dh5	4.007820137	1.98	0.99	2.2	0.23	457	1.066	111.1111111	11.61616162	9.565217391	50	0.3103448	Low Temp S2 Shoulder
489.4	Dh5	1.178781925	2	1.04	2.53	0.22	458	1.084	126.5	11	11.5	52	0.2913165	Low Temp S2 Shoulder
489.44	Dh5	3.742802303	1.83	1.13	1.92	0.24	458	1.084	104.9180328	13.1147541	8	61.74863388	0.3704918	Low Temp S2 Shoulder
489.48	Dh5	1.57116451	2.13	1.08	2.22	0.2	459	1.102	104.2253521	9.389671362	11.1	50.70422535	0.3272727	Low Temp S2 Shoulder
542.21	Dh5	0.472589792	4.71	1.56	4.16	0.18	461	1.138	88.32271762	3.821656051	23.11111111	33.12101911	0.2727273	Low Temp S2 Shoulder
542.265	Dh5	0.280373832	7.59	3.13	7.62	0.2	464	1.192	100.3952569	2.635046113	38.1	41.23847167	0.2911628	Low Temp S2 Shoulder
542.305	Dh5	1.227573182	5.43	1.97	5.93	0.19	461	1.138	109.2081031	3.49907919	31.21052632	36.27992634	0.2493671	Low Temp S2 Shoulder
542.38	Dh5	3.277060576	5.76	2.05	5.97	0.29	461	1.138	103.6458333	5.034722222	20.5862069	35.59027778	0.255611	Low Temp S2 Shoulder
542.44	Dh5	0.294117647	5.67	2.01	5.41	0.27	458	1.084	95.41446208	4.761904762	20.03703704	35.44973545	0.2708895	Low Temp S2 Shoulder
600.32	Dh5	3.297769156	6.36	2.31	5.57	0.21	468	1.264	87.57861635	3.301886792	26.52380952	36.32075472	0.2931472	Low Temp S2 Shoulder
600.35	Dh5	3.62745098	6.39	2.3	5.1	0.27	465	1.21	79.81220657	4.225352113	18.88888889	35.99374022	0.3108108	Low Temp S2 Shoulder
600.355	Dh5	5	6.93	3.14	6.76	0.25	463	1.174	97.54689755	3.607503608	27.04	45.31024531	0.3171717	Low Temp S2 Shoulder
600.37	Dh5	4.147031103	6.65	2.35	5.41	0.32	466	1.228	81.35338346	4.812030075	16.90625	35.33834586	0.3028351	Low Temp S2 Shoulder
600.4	Dh5	3.91221374	7.15	2.57	6.29	0.33	465	1.21	87.97202797	4.615384615	19.06060606	35.94405594	0.2900677	Low Temp S2 Shoulder
613.53	Dh5	1.133144476	8.91	2.66	8.4	0.27	468	1.264	94.27609428	3.03030303	31.11111111	29.85409652	0.2405063	Low Temp S2 Shoulder
613.57	Dh5	1.982160555	8.53	2.47	8.58	0.24	468	1.264	100.5861665	2.813599062	35.75	28.95662368	0.2235294	Low Temp S2 Shoulder
613.6	Dh5	3.80859375	8.88	3.01	7.53	0.38	463	1.174	84.7972973	4.279279279	19.81578947	33.8963964	0.2855787	Low Temp S2 Shoulder
613.64	Dh5	1.744186047	10.3	2.81	9.95	0.39	473	1.354	96.60194175	3.786407767	25.51282051	27.2815534	0.2202194	Low Temp S2 Shoulder
613.7	Dh5	2.032913843	11.7	3.5	10.14	0.35	469	1.282	86.66666667	2.991452991	28.97142857	29.91452991	0.2565982	Low Temp S2 Shoulder
613.725	Dh5	3.677932406	8.86	2.9	7.67	0.42	470	1.3	86.56884876	4.740406321	18.26190476	32.73137698	0.2743614	Low Temp S2 Shoulder
613.75	Dh5	1.857010214	9.05	2.63	8.07	0.25	470	1.3	89.17127072	2.762430939	32.28	29.06077348	0.2457944	Low Temp S2 Shoulder
613.78	Dh5	1.76744186	8.93	2.47	6.94	0.21	468	1.264	77.71556551	2.35162374	33.04761905	27.65957447	0.2624867	Low Temp S2 Shoulder
658.01	Dh5	4.956268222	1.37	0.24	0.49	0.08	466	1.228	35.76642336	5.839416058	6.125	17.51824818	0.3287671	
658.06	Dh5	2.367424242	1.42	0.23	0.46	0.1	464	1.192	32.3943662	7.042253521	4.6	16.1971831	0.3333333	
658.105	Dh5	2.027027027	1.19	0.21	0.39	0.12	461	1.138	32.77310924	10.08403361	3.25	17.64705882	0.35	
658.14	Dh5	3.021442495	1.35	0.24	0.52	0.12	464	1.192	38.51851852	8.888888889	4.333333333	17.77777778	0.3157895	
658.16	Dh5	2.799227799	1.34	0.2	0.42	0.1	463	1.174	31.34328358	7.462686567	4.2	14.92537313	0.3225806	
660.82	Dh2	6.960784314	6.11	2.3	5.57	0.28	467	1.246	91.16202946	4.582651391	19.89285714	37.64320786	0.292249	Low Temp S2 Shoulder
660.85	Dh2	6.14	8.40	3.13	7.54	0.24	467	1.25	89.76190476	2.857142857	31.41666667	37.26190476	0.2933458	Low Temp S2 Shoulder
660.88	Dh2	5.444126074	6.92	2.5	5.47	0.25	468	1.264	79.04624277	3.612716763	21.88	36.12716763	0.3136763	Low Temp S2 Shoulder
660.915	Dh2	4.875717017	8.19	3.49	7.45	0.39	472	1.336	90.96459096	4.761904762	19.1025641	42.61294261	0.3190128	Low Temp S2 Shoulder
660.93	Dh2	4.592314902	8.17	3.26	7.31	0.36	466	1.228	89.47368421	4.406364749	20.30555556	39.90208078	0.3084201	Low Temp S2 Shoulder
660.955	Dh2	5.044510386	7.73	3.3	6.79	0.35	471	1.318	87.83958603	4.527813713	19.4	42.69081501	0.3270565	
660.96	Dh2	3.773584906	10.7	4.3	10.84	0.37	465	1.21	101.3084112	3.457943925	29.2972973	40.18691589	0.2840159	Low Temp S2 Shoulder
660.99	Dh2	3.498542274	8.26	3.19	8.54	0.32	467	1.246	103.3898305	3.87409201	26.6875	38.61985472	0.2719523	Low Temp S2 Shoulder
674.08	Dh2	10.49562682	8.37	2.18	7.49	0.34	466	1.228	89.48626045	4.062126643	22.02941176	26.04540024	0.2254395	Low Temp S2 Shoulder
674.1	Dh2	9.783631232	9.95	2.77	10.02	0.34	466	1.228	100.7035176	3.417085427	29.47058824	27.83919598	0.2165754	Low Temp S2 Shoulder
674.14	Dh2	7.5	11.4	3.09	12.5	0.4	465	1.21	109.6491228	3.50877193	31.25	27.10526316	0.198204	Low Temp S2 Shoulder
674.15	Dh2	3.595080416	9.45	2.55	9.63	0.34	467	1.246	101.9047619	3.597883598	28.32352941	26.98412698	0.2093596	Low Temp S2 Shoulder
674.18	Dh2	6.597549482	11.6	3.02	12.27	0.44	466	1.228	105.7758621	3.793103448	27.88636364	26.03448276	0.1975147	Low Temp S2 Shoulder

Table 3 cont.		Values below detection limits are set at 1/2 the detection limit for plots. % Al in Dh5-658 plots are set at 12% where over the upper detection limit.																			
Sample Depth	Drill Hole	Se	Zn	Ga	As	Rb	Y	Sr	Zr	Nb	Mo	In	Sn	Sb	Te	Ba	La	Ce	Pr	Nd	Sm
		ppm 0.1	ppm 0.2	ppm 0.1	ppm 0.1	ppm 0.2	ppm 0.1	ppm 0.2	ppm 1	ppm 0.1	ppm 0.05	ppm 0.1	ppm 1	ppm 0.1	ppm 0.1	ppm 0.1	ppm 1	ppm 0.1	ppm 0.1	ppm 0.1	ppm 0.1
489.33	Dh5	2.4	142	15	22.1	129	20.5	146	141	20.6	2.3	0.1	3	0.5	<0.1	247	42.1	78.7	7.6	36.1	4.4
489.355	Dh5	2.9	132	24.6	16.1	165	25.4	150	161	37.4	2.26	<0.1	3	0.6	<0.1	62	39	76.6	9.8	38.4	6.6
489.4	Dh5	1.8	120	17.2	10.5	170	26.2	154	167	40.6	1.53	<0.1	3	0.5	<0.1	259	41.2	78.2	10	39.3	6.9
489.44	Dh5	2.4	159	24.8	23.1	163	26.6	160	164	38.4	2.91	<0.1	3	0.6	<0.1	55	39.2	77.5	10.1	39.6	7.2
489.48	Dh5	2.7	144	20	10.8	164	25.2	156	164	37.8	3.62	<0.1	3	0.6	<0.1	172	39.8	76.2	9.8	38.2	6.8
542.21	Dh5	4.8	87.6	25	35.1	158	33.5	145	161	26.7	5.85	<0.1	3	0.9	<0.1	47	36.8	69.4	9.6	38.1	7.1
542.265	Dh5	7.1	196	24	26.4	152	30.3	147	203	25.3	9.16	<0.1	3	1	<0.1	26	36.5	71.3	9.8	38.6	6.8
542.305	Dh5	4.6	137	23	25	131	26.4	141	178	26	4.88	<0.1	3	0.8	<0.1	74	33	58.6	8.4	33	5.9
542.38	Dh5	7.6	313	21.6	20.6	132	33.7	164	166	23.6	8.38	<0.1	3	0.9	<0.1	63	34.5	65.7	9.2	37.7	7.3
542.44	Dh5	4.6	273	22.1	38.1	123	34.1	158	179	24.7	5.74	<0.1	3	0.8	<0.1	68	36.2	66.7	9.6	38.8	7.4
600.32	Dh5	5.3	101	22.6	18.2	137	34.5	200	168	25.2	5.97	<0.1	3	1.3	<0.1	83	37.7	68.7	9.7	39	7.2
600.35	Dh5	6.2	99	17.4	18.4	79.6	26.7	153	82	11.6	5.98	<0.1	3	1.2	<0.1	63	35.9	63.6	8.9	34.7	6.4
600.355	Dh5	5.9	146	14.4	15.5	109	22.1	152	133	12.4	5.6	0.1	3	1.1	0.1	113	35.9	63.4	6.5	31.7	3.9
600.37	Dh5	5.7	98.7	17	16.1	80.4	26.9	162	77	11.4	5.13	<0.1	3	1	<0.1	66	35.7	63.8	9.2	35.4	6.7
600.4	Dh5	6.5	124	18.5	16.7	83.3	30.5	185	86	12	4.66	<0.1	3	1	<0.1	74	41.4	75.6	10.8	41.8	8
613.53	Dh5	11	171	22.2	20	123	37.3	241	161	23.3	4.24	<0.1	3	2	<0.1	38	35.2	61.4	9.4	37.4	7.1
613.57	Dh5	10	112	22.8	18.3	133	40.2	257	154	24.3	4.05	<0.1	3	1.8	0.2	53	38	66.4	10	40.3	7.5
613.6	Dh5	10.6	98	14.2	23.7	95.5	29	201	132	12.3	4.8	0.1	3	2	0.1	62	33.9	57.4	7	35.3	4.7
613.64	Dh5	11	349	24.2	21.1	137	36	273	169	25	5.49	<0.1	3	2.2	<0.1	42	38.7	68.3	10.1	40.1	7.4
613.7	Dh5	15	733	23.3	28.3	125	40.3	257	160	22.7	17.2	<0.1	3	2.6	<0.1	27	36.2	66.4	10.7	44	8.6
613.725	Dh5	9.2	173	14.7	14.3	100	20.7	183	128	12.5	4.4	0.1	3	1.7	0.1	139	34.1	52.6	6	28.5	3.3
613.75	Dh5	11.7	202	24.1	21.3	138	34.4	237	157	24.1	5.41	<0.1	3	2.2	<0.1	36	36.7	65.4	9.5	37.7	6.4
613.78	Dh5	12.8	224	23	24.8	122	40.2	227	151	22.8	4.96	<0.1	3	2.3	<0.1	33	33.6	61.6	9.5	39.5	7.6
658.01	Dh5	<0.1	130	21.7	22.6	153	25.3	166	183	30.7	1.34	<0.1	3	0.6	<0.1	147	34	74.8	8.8	34.6	6.6
658.06	Dh5	0.1	123	24.9	28.1	154	24.5	145	179	29.9	1.61	<0.1	3	0.7	<0.1	53	30.4	70.7	8.3	32.9	6.1
658.105	Dh5	0.8	130	25.5	21.9	144	24.9	163	174	30.2	1.47	<0.1	3	0.6	0.2	40	30.5	71.1	8.5	33.4	6.3
658.14	Dh5	<0.1	145	20.4	20.3	153	24.9	161	180	30	1.01	<0.1	3	0.6	<0.1	148	32.2	71.2	8.4	33.3	6.2
658.16	Dh5	<0.1	150	24.3	29.4	156	25.1	166	179	29.2	1.5	<0.1	3	0.6	0.1	46	30.4	69.6	8.3	33.4	6.3
660.82	Dh2	6.5	243	14.3	13.4	66	26.2	132	75	9.8	4.65	<0.1	3	1	<0.1	135	31.3	53.6	7.9	31.3	5.6
660.85	Dh2	8.3	166	16.8	19.3	63	25.9	129	91	11.2	5.6	<0.1	3	1.2	<0.1	61	31.5	53.7	7.7	30	5.7
660.88	Dh2	7.1	122	17.2	16.3	86.2	26.3	123	81	11.3	3.77	<0.1	3	1.2	<0.1	68	32.3	53.2	7.6	29.2	5.5
660.915	Dh2	7.7	227	13.3	15.1	96.3	24.6	135	136	11.6	4.9	<0.1	3	1.3	0.1	137	34.8	57.7	6.6	31.6	4
660.93	Dh2	8.9	122	16.6	46.8	75.3	27.6	128	81	11.3	5.6	<0.1	3	1.4	<0.1	57	33.3	55.5	8.2	31.3	5.9
660.955	Dh2	7.3	139	14.1	16.7	85.3	24.7	134	142	12.2	4.6	0.1	3	1.3	0.1	93	36.7	59.6	6.5	31.5	4
660.96	Dh2	11.8	523	17.1	29.2	84	26.4	132	87	10.6	6.45	<0.1	3	1.6	0.1	68	31	51.3	8.1	32.2	6
660.99	Dh2	8.2	151	18.2	18.3	87.2	27.8	126	79	11.3	5.27	<0.1	3	1.3	<0.1	85	32.9	51.7	8	31.4	5.8
674.08	Dh2	10.6	482	13.9	20.2	77	49.8	197	70	9	11.2	<0.1	3	2	<0.1	99	44.9	67.9	11.2	45	8.8
674.1	Dh2	11.3	363	13.7	18.5	64.2	42.6	167	66	8.9	11.6	<0.1	3	2.1	<0.1	83	38.7	58.1	9.7	38.5	7.7
674.14	Dh2	12.8	561	16.9	17.2	80.5	45.8	169	45	9.4	10.9	<0.1	3	2.1	<0.1	98	42.2	63	10.6	42.9	8.4
674.15	Dh2	12.6	246	15.4	19.6	84.8	37.9	147	74	10.3	9.08	<0.1	3	1.9	<0.1	66	39.4	62.6	10	40.1	8.2
674.18	Dh2	13.7	457	15.8	29.6	57.2	42.6	179	74	10.2	9.46	<0.1	3	2.1	<0.1	89	40.8	68.4	11.8	49.3	9.4

Table 3 cont.		Trace and Major Elements: ACT Labs. Lower detection limits listed below elements. Readings above and below detection limits are designated by > or < respectively.																					
Sample Depth	Drill Hole	Li	Na	Mg	Al	K	Ca	Cd	V	Cr	Mn	Fe	Hf	Hg	Ni	Er	Be	Ho	Ag	Cs	Co	Eu	Bi
		ppm	%	%	%	%	%	ppm	ppm	ppm	ppm	%	ppm	ppb	ppm	ppm	ppm	ppm	ppm	ppm	ppm	ppm	ppm
		0.5	0.01	0.01	0.01	0.01	0.01	0.1	1	0.5	1	0.01	0.1	10	0.5	0.1	0.1	0.1	0.05	0.05	0.1	0.05	0.02
489.33	Dh5	67.9	0.4	1.3	7.7	2.7	0.7	0.2	130	120	136	3.5	3.3	40	54.5	2.3	2.2	0.9	0.7	9.8	11.4	1.3	0.3
489.355	Dh5	101	0.57	1.47	8.91	3.27	0.64	0.3	138	137	142	3.66	6.9	< 10	59.8	2.9	3.2	1	0.74	9.94	10.8	1.27	0.3
489.4	Dh5	105	0.6	1.53	9.38	3.38	0.63	0.3	144	159	152	3.24	7.2	< 10	48.9	2.9	3.2	1	0.64	10.4	9.7	1.29	0.3
489.44	Dh5	96.1	0.6	1.47	9.06	3.23	0.67	0.4	137	116	123	4	6.9	30	60.7	2.9	3.1	1	0.68	9.79	11.4	1.35	0.28
489.48	Dh5	96.9	0.64	1.35	8.99	3.23	0.45	0.4	136	132	125	3.09	7	70	58.6	2.8	2.9	0.9	0.75	9.87	10.5	1.24	0.29
542.21	Dh5	63.4	0.53	1.06	9.09	3.67	0.39	0.7	159	132	93	3.41	6.7	10	70.6	3.4	3.2	1.2	0.75	9.22	10.2	1.44	0.28
542.265	Dh5	67.6	0.52	0.95	8.68	3.44	0.22	2.5	170	198	104	3.94	7.6	70	91.6	3.3	2.9	1.1	1.72	8.76	10.2	1.3	0.32
542.305	Dh5	64.4	0.51	0.97	9.22	3.04	0.3	1.2	162	185	96	2.91	6.9	60	62.5	2.8	3.2	0.9	1.22	8.41	9	1.17	0.3
542.38	Dh5	63.3	0.5	1.04	7.91	3.11	0.43	5.2	139	166	146	3.48	6.6	80	77.2	3.4	2.5	1.2	1.83	7.97	8.8	1.43	0.29
542.44	Dh5	61.6	0.52	0.94	8.73	2.72	0.29	4.1	146	181	89	3.09	6.9	50	66.9	3.5	2.8	1.2	1.27	7.96	9.5	1.39	0.28
600.32	Dh5	70	0.51	1.03	9.31	3.1	0.5	0.4	167	166	107	2.46	6.9	50	63.8	3.5	3.2	1.2	1.22	8.81	8.4	1.34	0.27
600.35	Dh5	74	0.39	0.93	8.12	2.09	0.39	0.5	161	111	102	2.67	3.6	50	71.1	3.2	2.9	1	2	8.82	7.5	1.27	0.28
600.355	Dh5	41.3	0.3	0.8	7.2	2.9	0.4	0.6	143	118	157	2.6	2.9	100	70.3	2.4	1.9	0.9	1.1	8.3	9.1	1.2	0.3
600.37	Dh5	73.9	0.38	0.88	7.57	2.04	0.38	0.5	160	105	91	2.59	3.5	60	66.2	3.1	2.8	1	1.5	8.8	7	1.3	0.27
600.4	Dh5	80.5	0.4	0.91	7.9	2.24	0.37	0.7	170	116	97	2.49	3.6	50	71.5	3.4	2.9	1.1	1.53	9.58	7.5	1.54	0.28
613.53	Dh5	70.4	0.47	0.94	8.44	2.8	0.42	1.4	268	178	103	2.88	6.4	70	71	3.7	3.1	1.2	1.8	8.34	8.1	1.35	0.27
613.57	Dh5	73.7	0.48	1.03	9.02	2.89	0.47	0.7	275	129	108	2.44	6.2	50	65.4	3.9	3.2	1.4	1.61	8.77	7.8	1.48	0.27
613.6	Dh5	45.1	0.3	0.8	6.7	2.6	0.4	0.6	228	136	94	2.9	2.9	150	77.5	2.9	2.1	1.1	2	7.6	8.4	1.5	0.3
613.64	Dh5	77.5	0.48	1.04	9.26	2.95	0.36	3.8	305	159	118	2.49	6.6	< 10	86.5	3.7	3.3	1.2	2.6	9.13	9	1.36	0.29
613.7	Dh5	71.7	0.45	0.93	8.2	2.69	0.39	9.6	278	189	111	3.11	6.1	20	152	3.9	3.2	1.4	3.13	8.06	10.1	1.63	0.28
613.725	Dh5	46.1	0.3	0.7	7.2	2.8	0.3	1.4	237	135	91	2	2.9	110	70.2	2.2	2.1	0.8	1.8	8.4	8.6	1	0.3
613.75	Dh5	75	0.46	0.97	8.95	2.95	0.34	1.8	266	144	72	2.7	6.2	100	81.4	3.5	3.3	1.2	2.05	9.11	9.1	1.22	0.29
613.78	Dh5	71	0.44	0.92	8.7	2.73	0.37	2.7	258	173	73	3.14	6.1	130	82	3.9	3.2	1.3	2.11	8.2	8.4	1.51	0.28
658.01	Dh5	128	0.57	1.18	> 10.0	2.96	0.33	0.1	173	71.1	169	3.6	7.7	120	47.1	2.9	3.2	1	0.86	10.6	11	1.19	0.45
658.06	Dh5	126	0.57	1.17	> 10.0	3.16	0.33	< 0.1	168	79.8	208	4.48	7.7	130	53.9	2.8	3	0.9	0.69	10.1	11.3	1.15	0.44
658.105	Dh5	123	0.55	1.17	> 10.0	2.79	0.34	0.1	166	74	233	4.43	7.6	180	49.4	2.8	3.3	0.9	0.72	9.86	10.4	1.15	0.44
658.14	Dh5	125	0.55	1.16	9.98	3.06	0.33	0.2	167	89	151	3.27	7.6	60	37.7	2.9	3.2	1	0.55	9.87	10.4	1.17	0.43
658.16	Dh5	126	0.56	1.16	> 10.0	3.14	0.34	0.2	159	85.6	197	4.41	7.5	150	55.2	2.8	3.1	1	0.53	9.68	12.1	1.13	0.41
660.82	Dh2	80.6	0.38	0.92	6.38	1.63	0.76	1.8	163	104	128	2.31	3.2	70	57.2	2.8	2.1	1	1.98	6.2	5.9	1.18	0.2
660.85	Dh2	79.5	0.34	0.87	6.72	1.62	0.59	1.2	187	122	116	2.57	3.5	110	71.7	2.9	2.5	0.9	2.34	7.17	6.9	1.12	0.27
660.88	Dh2	76.7	0.37	0.89	6.96	2.58	0.59	0.7	192	118	106	2.43	3.3	20	55.3	2.8	2.4	0.8	1.27	7.87	6.8	1.09	0.28
660.915	Dh2	48.7	0.3	0.8	6.9	2.6	0.7	1.5	170	135	111	2.35	3	100	67.3	2.5	1.8	1	2.1	6.95	7.8	1.25	0.3
660.93	Dh2	78.7	0.33	0.86	6.89	1.95	0.57	0.8	198	120	118	2.93	3.3	110	71.1	3	2.7	0.9	2.57	7.61	7.5	1.15	0.27
660.955	Dh2	50.9	0.3	0.9	7.2	2.1	0.7	0.8	174	141	118	2.5	3.1	100	65.5	2.7	2	1	1.8	7.2	8.1	1.3	0.3
660.96	Dh2	81.3	0.32	0.82	6.75	2.54	0.54	5.7	207	132	99	2.65	3.4	60	90.7	3	2.5	0.9	3.89	7.14	6.9	1.17	0.27
660.99	Dh2	83.1	0.35	0.81	7.02	2.67	0.53	1	212	132	115	2.35	3.3	80	70.7	3	2.7	1	3.08	8.03	7	1.16	0.29
674.08	Dh2	58.8	0.38	1.3	5.91	2.11	1.94	6.8	271	108	163	2.36	2.9	40	84.5	4.8	2.2	1.5	2.81	6.19	6	1.81	0.21
674.1	Dh2	54	0.34	1.08	5.67	1.84	1.59	5.3	275	113	149	2.06	2.6	50	88	4.2	2.2	1.3	3.87	5.85	5.8	1.55	0.24
674.14	Dh2	61	0.37	1.04	6.99	2.24	1.24	9	336	147	121	2.08	0.9	50	103	4.5	2.6	1.5	4.41	7.44	6.5	1.68	0.27
674.15	Dh2	63.8	0.37	0.78	6.76	2.35	0.74	3	303	124	112	2.24	3.1	40	93.3	4	2.8	1.2	3.28	7.67	6.7	1.52	0.26
674.18	Dh2	63.7	0.36	0.87	6.13	1.54	1	6.6	310	128	128	2.34	3.1	20	99.2	4.3	2.8	1.4	4	7.19	6.3	1.9	0.28

Table 3 cont.		Gd	Tb	Dy	Cu	Ge	Tm	Yb	Lu	Ta	W	Re	Tl	Pb	Sc	Th	U	Ti	P	S
Sample	Drill Hole	ppm	ppm	ppm	ppm	ppm	ppm	ppm	ppm	ppm	ppm	ppm	ppm	ppm	ppm	ppm	ppm	%	%	%
Depth		0.1	0.1	0.1	0.2	0.1	0.1	0.1	0.1	0.1	0.1	0.001	0.05	0.5	1	0.1	0.1	0.0005	0.001	0.01
489.33	Dh5	5.1	0.7	3.8	53.6	<0.1	0.3	2.3	0.4	1.1	1.1	<0.001	0.7	21.7	18	12.5	4.2	0.56	0.058	1.53
489.355	Dh5	4.9	0.7	4.8	49.2	<0.1	0.4	2.9	0.4	3.4	4.7	0.003	0.84	19.3	19	11.3	3.4	0.551	0.053	1.59
489.4	Dh5	5	0.8	5	45.8	<0.1	0.4	3	0.4	3.7	2.4	<0.001	0.81	19.5	20	12.5	3.4	0.599	0.057	0.99
489.44	Dh5	5.3	0.8	5.1	49.2	<0.1	0.4	2.9	0.4	3.5	2.5	0.006	0.85	19.8	18	10.5	3.5	0.533	0.054	1.98
489.48	Dh5	4.8	0.7	4.7	52.8	<0.1	0.4	2.9	0.4	3.3	2.2	0.005	0.85	18.4	17	11.8	3.4	0.529	0.049	1.1
542.21	Dh5	5.9	0.9	5.9	55.4	<0.1	0.5	3.3	0.5	2.7	2.2	0.007	1.06	19.4	17	10.4	5	0.52	0.079	2.57
542.265	Dh5	5.2	0.8	5.4	72	<0.1	0.5	3.3	0.5	2.6	1.8	0.015	1.43	23.9	17	9.7	5.5	0.499	0.058	3.26
542.305	Dh5	4.6	0.7	4.6	52.4	<0.1	0.4	2.8	0.4	2.6	2	0.009	0.99	18.6	17	8.3	4.1	0.516	0.061	1.97
542.38	Dh5	5.9	0.9	5.8	62.5	<0.1	0.5	3.3	0.5	2.4	1.7	0.022	1.36	20.2	15	8.7	4.9	0.498	0.081	2.43
542.44	Dh5	5.8	0.9	5.9	51.7	<0.1	0.5	3.3	0.5	2.5	2	0.016	1.14	18.7	17	9.1	4.5	0.534	0.079	2.36
600.32	Dh5	5.5	0.9	5.6	42.7	<0.1	0.5	3.6	0.5	2.5	1.9	0.017	0.79	15.9	17	10.3	5.1	0.566	0.085	1.88
600.35	Dh5	5.5	0.8	5.1	52.9	<0.1	0.5	3	0.6	0.9	1.4	0.022	0.95	18.2	14	11	5.4	0.524	0.071	2.52
600.355	Dh5	4.9	0.7	3.8	51.1	<0.1	0.3	2.3	0.4	0.8	0.9	<0.001	0.7	17.7	15	9.7	3.7	0.527	0.068	2.31
600.37	Dh5	5.7	0.8	5	46.9	<0.1	0.5	2.9	0.5	0.8	1.2	0.022	0.77	17.7	14	11.1	5.4	0.509	0.067	2.29
600.4	Dh5	6.7	0.9	5.8	52.5	<0.1	0.5	3.1	0.5	0.8	1.2	0.028	0.83	18.5	14	12.5	6	0.524	0.068	2.08
613.53	Dh5	5.8	0.9	6.1	62.8	<0.1	0.5	3.5	0.5	2.3	1.9	0.016	0.71	18.5	17	8.9	4.9	0.539	0.091	2.84
613.57	Dh5	6.4	0.9	6.5	53.7	<0.1	0.6	3.8	0.6	2.4	2	0.013	0.75	19	17	9.9	5.5	0.544	0.098	2.16
613.6	Dh5	6.3	0.9	4.8	60.8	<0.1	0.3	2.5	0.4	0.7	1	<0.001	0.6	19.3	14	7.2	4	0.507	0.103	3.07
613.64	Dh5	5.7	0.8	5.8	63.1	<0.1	0.5	3.7	0.6	2.5	2	0.032	1.02	19	18	10.1	6	0.591	0.068	2.42
613.7	Dh5	6.8	1	6.7	81.4	<0.1	0.6	3.6	0.5	2.3	1.9	0.038	1.59	19.2	16	9	6.1	0.521	0.078	3.2
613.725	Dh5	4	0.6	3.2	59	<0.1	0.3	2.2	0.4	0.7	1	<0.001	0.7	20.7	15	7.9	3.5	0.548	0.053	1.87
613.75	Dh5	5.1	0.8	5.5	57.7	<0.1	0.5	3.6	0.6	2.4	1.9	0.019	0.81	20.5	17	9.8	5.7	0.531	0.058	2.49
613.78	Dh5	6.4	1	6.5	56.8	<0.1	0.5	3.6	0.5	2.3	1.9	0.015	0.87	20.1	16	8.1	5	0.524	0.082	3.13
658.01	Dh5	4.6	0.7	4.8	34.7	<0.1	0.4	3	0.5	2.9	2.5	<0.001	0.77	24.6	18	11.5	3.2	0.593	0.052	1.35
658.06	Dh5	4.3	0.7	4.6	38.2	<0.1	0.4	2.9	0.4	2.9	2.3	<0.001	0.83	25.4	18	8.9	3.2	0.573	0.05	2.3
658.105	Dh5	4.5	0.7	4.7	40.5	<0.1	0.4	2.9	0.4	2.9	2.3	0.003	0.8	21.6	19	8.5	3.2	0.602	0.053	2.46
658.14	Dh5	4.4	0.7	4.6	36.7	<0.1	0.4	2.9	0.4	2.9	2.2	0.006	0.8	20.3	19	11.2	3.2	0.64	0.057	1.04
658.16	Dh5	4.6	0.7	4.7	37	<0.1	0.4	3	0.4	2.8	2	0.004	0.84	22.7	18	8.7	3.1	0.595	0.054	2.32
660.82	Dh2	5.3	0.8	4.6	47.7	<0.1	0.4	2.6	0.5	0.7	1.1	0.02	0.77	14.4	14	10.4	4.8	0.455	0.073	1.75
660.85	Dh2	5	0.7	4.5	62.7	<0.1	0.4	2.7	0.5	0.8	1.2	0.027	0.92	18.3	14	9.6	4.8	0.502	0.063	2.18
660.88	Dh2	4.8	0.7	4.4	56.2	<0.1	0.4	2.7	0.5	0.8	1.3	0.016	0.69	18.4	14	10.5	4.2	0.507	0.068	1.91
660.915	Dh2	5	0.7	4.1	67.3	<0.1	0.3	2.5	0.4	0.8	0.9	<0.001	0.8	16.8	14	9.5	3.8	0.492	0.081	1.98
660.93	Dh2	5.2	0.8	4.7	66.8	<0.1	0.5	2.9	0.5	0.8	1.2	0.022	0.85	18.4	14	9.4	4.9	0.487	0.071	2.58
660.955	Dh2	5.1	0.7	4.2	58.4	<0.1	0.3	2.5	0.4	0.8	1	<0.001	0.7	19.1	15	9.5	3.8	0.513	0.079	2.18
660.96	Dh2	5.4	0.7	4.7	81.8	<0.1	0.4	2.8	0.5	0.7	1.2	0.036	1.54	17.5	13	9.3	4.6	0.469	0.06	2.42
660.99	Dh2	5.5	0.8	4.9	66.3	<0.1	0.4	2.7	0.5	0.8	1.3	0.028	0.84	18.6	13	8.7	3.7	0.498	0.071	1.88
674.08	Dh2	8.5	1.2	7.6	56.7	<0.1	0.7	4.1	0.8	0.7	1.2	0.04	1.66	14.8	15	11.1	10.2	0.408	0.203	2.16
674.1	Dh2	7.3	1	6.5	71.1	<0.1	0.6	3.7	0.7	0.7	1.1	0.042	1.61	15	15	9.3	9.2	0.426	0.188	2.09
674.14	Dh2	8	1.2	7.1	83.3	<0.1	0.7	4	0.7	0.5	1.3	0.052	1.84	16.8	15	11	9.8	0.455	0.168	1.9
674.15	Dh2	7	1	6.3	69.5	<0.1	0.6	3.5	0.6	0.7	1.3	0.043	1.2	18.3	14	10.3	7.4	0.479	0.141	2.32
674.18	Dh2	9	1.3	7.5	77.6	<0.1	0.6	3.5	0.6	0.7	1.2	0.049	1.32	17.1	15	11.4	15	0.473	0.159	2.34

Table 3 cont.		Stable Isotopes: IsoAnalytical						
Sample Depth	Drill Hole	d13CV-PDB	d18OV-PDB	d13CV-PDB	Elemental N	d15NAir	Elemental Sulphur (%)	d34SV-CDT
		(‰)	(‰)	(‰)	(‰)	(‰)	(%)	(‰)
489.33	Dh5							
489.355	Dh5							
489.4	Dh5	-8.35	-8.92	-29.63	0.18	3.42	0.99	-18.43
489.44	Dh5			-29.71	0.17	3.46	2.10	-28.17
489.48	Dh5							
542.21	Dh5	-7.17	-7.99	-26.89	0.22	3.48	2.71	-29.03
542.265	Dh5							
542.305	Dh5							
542.38	Dh5			-26.95	0.25	3.43	2.55	-26.40
542.44	Dh5							
600.32	Dh5							
600.35	Dh5							
600.355	Dh5							
600.37	Dh5	-7.33	-10.06	-26.21	0.25	4.82	2.60	-22.39
600.4	Dh5	-8.08	-9.49	-26.44	0.27	4.56	2.32	-21.79
613.53	Dh5							
613.57	Dh5							
613.6	Dh5							
613.64	Dh5	-8.83	-12.23	-25.81	0.35	3.99	2.29	-15.95
613.7	Dh5							
613.725	Dh5							
613.75	Dh5	-7.61	-10.45	-25.96	0.31	4.27	2.65	-11.91
613.78	Dh5	-9.20	-12.03	-25.91	0.32	4.28	3.46	-7.37
658.01	Dh5			-25.25	0.16	3.62	1.34	-33.49
658.06	Dh5							
658.105	Dh5	-9.26	-9.79	-25.26	0.16	3.26	2.32	-27.76
658.14	Dh5							
658.16	Dh5							
660.82	Dh2	-9.42	-12.11	-26.01	0.22	4.52	1.84	-13.53
660.85	Dh2							
660.88	Dh2							
660.93	Dh2							
660.955	Dh2							
660.96	Dh2	-9.56	-12.89	-26.06			2.81	-16.53
660.99	Dh2							
674.08	Dh2	-13.58	-14.54	-26.36	0.30	4.92	2.43	-17.03
674.1	Dh2							
674.14	Dh2							
674.15	Dh2	-11.80	-13.92	-26.24	0.34	4.77	2.56	-16.73
674.18	Dh2							

APPENDIX B

Table 4-Re-Os Total Analytical Blank Data

<b>Blank ID</b>	<b>Re Blank</b>	<b>err (2-s)</b>	<b>Blank % Error</b>	<b>Os Blank</b>	<b>err (2-s)</b>	<b>Blank % Error</b>	<b>Blank comp</b>	<b>err (2-s)</b>
<b>A</b>	6.781	0.056351	0.831003	0.277008	0.004368	1.57677	0.784472	0.010588
<b>B</b>	11.208	0.092217	0.822783	0.277008	0.004368	1.57677	0.784472	0.010588
<b>C</b>	58.818	0.308441	0.524402	0.108	0.016	14.81481	0.225	0.102
<b>D</b>	61.532	0.105538	0.171517	0.321305	0.010668	3.320259	1.025162	0.019333
<b>E</b>	59.125	0.459891	0.77783	0.210274	0.006978	3.318619	2.104842	0.051292
<b>F</b>	56.979	22.46991	39.43562	0.209298	0.237773	113.6051	0.212467	0.108018
<b>G</b>	58.756	0.161245	0.27443	0.193091	0.005116	2.649584	0.286787	0.00744
<b>H</b>	53.13	0.269061	0.506419	0.189874	0.002383	1.255033	0.737742	0.007401
<b>I</b>	59.939	0.197055	0.328759	0.167808	0.004576	2.726737	0.287742	0.006441

## APPENDIX C: RE-OS ISOCHRONS

